

# Stellar evolution along the AGB as revealed by the shape of Miras' visual light curves

*D.T. Hoai, P.T. Nhung, P. Darriulat and M.N. Tan*  
*Department of Astrophysics, VNSC/VAST, 18 Hoang Quoc Viet, Ha Noi, Viet Nam*

## Abstract

A new analysis of a sample of visual light curves of Long Period Variable (LPV) Mira stars is presented. The curves cover the past four decades and are selected from the AAVSO data base as including a very large number of high-density and high-quality observations. The aim of the analysis is to offer a more precise, more quantitative and more systematic picture than available from earlier studies. The results corroborate earlier descriptions and reveal new correlations between the shapes of the light curves and the time spent by the star on the Asymptotic Giant Branch (AGB). A family of nearly sinusoidal curves, associated with M-type spectral types and displaying no sign of having entered the thermally-pulsing phase (TP-AGB) is identified with good confidence. All other curves are clearly distinct from this family and usually start departing from it by displaying a broader luminosity minimum, implying a slowing down of the rate of luminosity increase on the ascending branch. This slowing down feature, referred to as a hump, spans across the ascending branch as the spectral-type of the star evolves from M to C. It may go all the way to maximal light or stop earlier, covering only part of the ascending branch. While this general average trend is established with good confidence, deviations from it cause a significant scatter of the parameters defining the shapes of the curves. Comments aimed at shedding light on the underlying physics are presented together with speculative interpretations, in the hope that they could encourage and inspire new studies, in particular based on simulations using state-of-the-art models of the inner star dynamics.

## 1. Introduction

For centuries, some stars have been known to display variable apparent visual luminosity, some of which pulsating regularly. Such are, for example, the Cepheids and the Long-Period Variables (LPV) on the Asymptotic Giant Branch (AGB). The former were discovered at the end of the XVIIIth century (Pigott 1785, Goodricke 1786) while the first pulsating AGB star, *o* Ceti, was observed by Fabricius at the end of the XVIth century (Hoffleit 1997). Over time, stars displaying similar variability, with periods at the scale of a few days for the former and of a year for the latter, have been discovered; they are now known as Cepheids and Miras respectively and the brighter of both families have been the targets of high-quality observations for many decades, often over a century. In the early years of the XXth century, Henrietta Leavitt discovered the period-luminosity relation obeyed by Cepheids in the Magellanic Clouds, for which the distance to Earth is well-defined (Leavitt 1908 & 1912), and Eddington proposed a mechanism governing their pulsation, which is now commonly accepted and is known under the name of kappa-mechanism (Eddington 1917).

The kappa-mechanism implies a specific dependence of the opacity  $\kappa$  (kappa) of the star interior as a function of density  $\rho$  and temperature  $T$ . When energy transport is purely radiative,  $\kappa$  obeys approximately the Kramers law,  $\kappa \sim \rho T^{-7/2}$ , which accounts for both bound-free and free-free photon absorption (ionisation and bremsstrahlung, respectively). A small contraction causes both  $\rho$  and  $T$  to increase but the effect of the latter on opacity dominates over that of the former, allowing for more photons to escape: the star is in a state of stable equilibrium, the effects of temperature and pressure balancing each other. However, as Eddington remarked, if the opacity increases with temperature, the star becomes unstable against pulsations; but it was not until the middle of the century that Zhevakin (1953) identified ionised helium as the cause of the anomalous behaviour of the opacity. What happens is that the heat generated by compression is mostly used to ionise the medium and the temperature remains essentially constant as the density increases. Such a kappa-mechanism is at work in a region of the Hertzsprung-Russel (HR) diagram known as the instability strip and explains reasonably well the pulsations of Cepheids (Guzik et al. 2023 and references therein).

In contrast, for AGB stars, the energy transport is dominantly convective rather than radiative, and

therefore essentially independent of the opacity. A description of their pulsations cannot be as straightforward as in the case of Cepheids: to explain the pulsating instability in AGB stars one needs a dynamic theory of convection, for which a one-dimensional approximation, the so-called Mixing Length Theory (MLT), has been in use for over six decades (Joyce & Tayar 2023 and references therein). In analogy with molecular heat transfer, it describes the bulk movement of the fluid in terms of the mean-free path of parcels in pressure equilibrium, but not in thermal equilibrium, with their surroundings, governed by the dependence of pressure on temperature. Recently, significant progress toward producing more realistic three-dimensional models of convection has been achieved (Andrassy et al. 2022 and references therein, Rizzuti et al. 2024 and references therein) and the role played by convective cells in the evolution of AGB stars has become an important topic of study, both for observations (Rosales-Guzmán et al. 2024, Paladini et al. 2018, Darriulat et al. 2024) and for modelling (Herwig 2005, Marigo et al. 2013 and references therein, Freytag and Höfner 2023 and references therein).

Another major complication makes the study of the light curves of LPV AGB stars particularly difficult: dust is abundantly produced in the cool atmospheres of the stars and, together with pulsations, is the main driver, by radiation pressure from the stellar surface, of the mass-losing wind (Liljegren et al. 2016 and references therein, McDonald et al. 2018). As noted by Reid and Goldston (2002) for oxygen-rich stars and by Winters et al. (1994) for carbon-rich stars, such dust significantly hides the observation of the photosphere in the visible and dramatically affects the appearance of the visual light curve.

In spite of such difficult interpretation, much effort has been dedicated to the study of the visual light curves of LPV AGB stars, with the aim to relate the main features that they display to properties specific to the pulsating star. In particular, the very long intervals of time over which such curves have been observed, often over a century, have allowed for precise measurements of the pulsation period and for revealing its evolution with time. Fourier transforms and wavelet techniques are commonly used for such studies (Templeton et al. 2005). Period-luminosity relations have been identified (McDonald and Zijlstra 2016 and references therein, Whitelock et al. 2008, Soszynski et al. 2007), showing evidence for Miras to be radial pulsators in the fundamental mode (Wood & Sebo 1996). Particular attention has been given to the study of period changes over time. Zijlstra & Bedding (2002) distinguish between three different types of period changes: continuous evolution, sudden changes and meandering periods. Indeed, strong period changes have been observed in a small fraction of Miras (Schwarzschild and Härm 1967, Templeton et al. 2005 and references therein, Wood & Zarro 1981, Gal & Szatmary 1995, Hawkins et al. 2001, Zijlstra et al. 2002, Merchán Benítez and Jurado Vargas, 2000 & 2002, Uttenthaler et al. 2011 and 2016a & b, Molnár et al. 2019) and are often, but not always, interpreted as evidence for recent thermal pulses in the helium burning shell. Correlations between the phase, traditionally measured from the maxima of the visual light curves and spanning one unit over a period, and temperature or diameter of the pulsating star have been measured in the near infrared in a few cases (Woodruff et al. 2008, Lacour et al. 2009, Van Belle et al. 1996, 2002); the temperature is found to be anti-correlated with the star diameter, as is also the case for Cepheids (Andrievsky et al. 2005), but important dependence of the luminosity on wavelength makes a reliable interpretation of these observations difficult.

More generally, the indicators of the evolution of LPVs along the AGB, in particular those that reveal the past occurrence of a third-dredge-up event, are found to be correlated not only with the period, but with several other features of the light curves. Such is the case of the  $^{12}\text{C}/^{13}\text{C}$  ratio (Ohnaka & Tsuji 1996, Abia & Isern 1997, Greaves & Holland 1997, Schöier & Olofsson 2000, Ramstedt & Olofsson 2014, Lebzelter et al. 2019), of the presence of technetium in the spectrum (Uttenthaler et al. 2019 and references therein), of the transition from oxygen-rich to carbon-rich (Mennessier et al. 1997, Whitelock 1999). Similarly, in the case of more massive stars, the occurrence of hot bottom burning (García-Hernández et al. 2013 and references therein) has been found to be correlated with peculiarities of the light curves. Other, weaker correlations, mostly related to the chemistry of the star atmosphere, have been reported: between OH emission and the steepness of the rising branch of the visual light curve (Bowers 1975, Bowers & Kerr 1977); between the appearance at 9.7 and 20 microns of silicate emission features (Vardya et al. 1986, Onaka et al. 1989), or also the dust mass loss rate evaluated using the K-[22] colour index (Merchán Benítez et al. 2023) and the asymmetry of the light

oscillation; between the detection of the H<sub>2</sub>O vapour line at 1.35 cm (Vardya et al. 1987), or also of dust formation (Le Bertre 1992, Winters et al. 1994), and the shape of the oscillation.

Several authors, faced with the difficulty to devise a reliable and sensible interpretation of the visual light curves of Mira stars, have attempted to produce classifications in terms of the particular features that they display. It started early in the past century with Ludendorff (1928) making a distinction between three main types of light curves: ( $\alpha$ ), when the ascending branch is steeper than the descending branch and the minimum broader than the maximum; ( $\beta$ ), when the curve is essentially symmetric with only minor differences between the steepness of the ascending and descending branches; and ( $\gamma$ ), when the ascending branch displays steps or humps, or when the oscillations are double-peaked. Indeed, the asymmetry between ascending and descending branches and the possible lack of linearity of the former, usually in the form of humps<sup>1</sup>, are, together with the amplitude of the oscillations, major features that have been the object of detailed consideration in all studies. Similar, but slightly different features have been observed in the near-infrared (e.g. Lockwood and Wind 1971), suggesting that they are indicators of intrinsic properties of the pulsating star. Subsequently, attempts at making the Ludendorff classification less subjective and at quantifying the relevant features by introducing adequate parameters have been made; in particular, Vardya (1988) introduced the asymmetry parameter  $f$ , defined as the ratio of the rising time over the period, and found that 80% of the Mira stars lie in the range  $0.4 < f < 0.5$  and that  $f$  is correlated with the M, S or C spectral type of the pulsating star. Lebzelter (2011) has parameterised the mean deviation of the oscillation profile from a sine wave on the ascending and descending branches separately, making a distinction between light curves displaying a broad minimum and a narrow maximum, and light curves displaying a narrow minimum and a broad maximum. More recently, Merchán Benítez et al. (2023) have separated Mira stars in two classes depending on both the symmetry and linearity of the shape of the oscillations and found a clear correlation with the dust mass-loss rate evaluated using the K-[22] colour index.

The study reported in the present article is in the wake of the work of these latter authors, motivated as we are by the feeling that the outstanding set of high-quality observations of visual light curves of LPV AGB stars has not yet been exploited as thoroughly as it deserves. Yet, we are conscious of the difficulty that such a study is facing and of the quantity and quality of previous investigations sharing the same ambition: we have defined accordingly which method to use and which sample of stars to study.

The article is organised as follows: in the next two sections we define the samples of curves on which the analysis is based and the parameterisation used to characterise each curve. Reaching reliable conclusions with confidence implies severe restrictions on the quality and density of the observations from which the curves are made. For this reason, we present analyses of two separate samples of light curves, one referred to as sample A is larger but the curve parameters are less rigorously defined than for the other, smaller sample, referred to as sample B. Sample A includes 71 stars and the curve parameters are simply evaluated from the plots accessible from the AAVSO website, without resorting to the detailed observational data stored in the AAVSO data base. Sample B includes only 32 curves but uses as input the observational data of the AAVSO data base, allowing for a rigorous definition of the relevant parameters. Section 4 discusses the main results obtained for oxygen-rich stars and Section 5 for carbon stars. Section 6 comments on the regularity of the light curves and Section 7 presents a discussion of the results attempting to correlate the properties of the light curves with the evolution of the star along the AGB. A brief summary is presented in Section 8.

## 2. Selection of visual light curves

Any progress in the understanding and interpretation of the visual light curves of Mira stars must build on, rather than repeat, results obtained by earlier studies (Ludendorff 1928, Vardya 1988, Lebzelter 2011, Merchán Benítez et al. 2023). These studies identified several basic properties of such curves that help with their characterisation: the asymmetry between the ascending and descending branches, the irregularity between successive oscillations, both in time and magnitude, the width of the maxima and minima, the possible occurrence of non-linear features on the ascending branch, usually in the form of humps. They give evidence

---

<sup>1</sup> These describe episodes of slowing down of the rate of luminosity increase on the ascending branch of an oscillation. They last a fraction of a period, typically 10 to 15%. They are usually referred to as *bumps* or *humps* in the published literature and we use the latter in the present article.

for correlations between the shape of the curve and the stage of evolution of the pulsating star on the AGB, possibly revealing the occurrence of recent helium flashes and third-dredge-up events, and making a distinction between stars of M, S and C spectral types. In the wake of such findings, the present study aims at providing a more precise and more detailed description of the shapes of the curves in the hope to better understand their relation to the intrinsic properties of the pulsating star. This requires restricting the study to light curves made from measurements of outstanding density and quality, implying that one must accept to work on relatively small samples, giving up the ambition to cover as much as possible of the available observations. Such an approach has guided the work reported in the present article. It has been arbitrarily restricted to observations covering the forty past years and to visual light curves from the AAVSO data base, with the understanding that curves from other sources and different wavelengths could be considered at a later stage if judged necessary. More precisely, we select stars from the sample used by Merchán Benítez et al. (2023), covering 548 Mira stars with light curves of reasonable quality having a full V-band amplitude in excess of 2.5 mag. Such a sample provides a good coverage of the Mira family, however with the exception of binaries, which Merchán Benítez et al. considered judicious to exclude; such are the cases of *o* Ceti and R Aqr. For each star of the sample, Merchán Benítez et al. (2023) provide the following information: the spectral type, the period and its variability, the possible presence of technetium in the spectrum, the  $^{12}\text{C}/^{13}\text{C}$  ratio when available, the values of the colour indices (in units of magnitude)  $K-[22]$  and  $[3.4]-[22]$ , both of which are commonly used proxies of the dust mass-loss rate (McDonald et al. 2016, 2018). In addition, they list the class, S (for symmetric) or A (for antisymmetric), to which they assign the curve. Class A includes curves displaying a hump or a sharp change of slope on their ascending branch; class S includes all other curves. Figure 1 displays the distribution of the curves in the colour vs period planes.

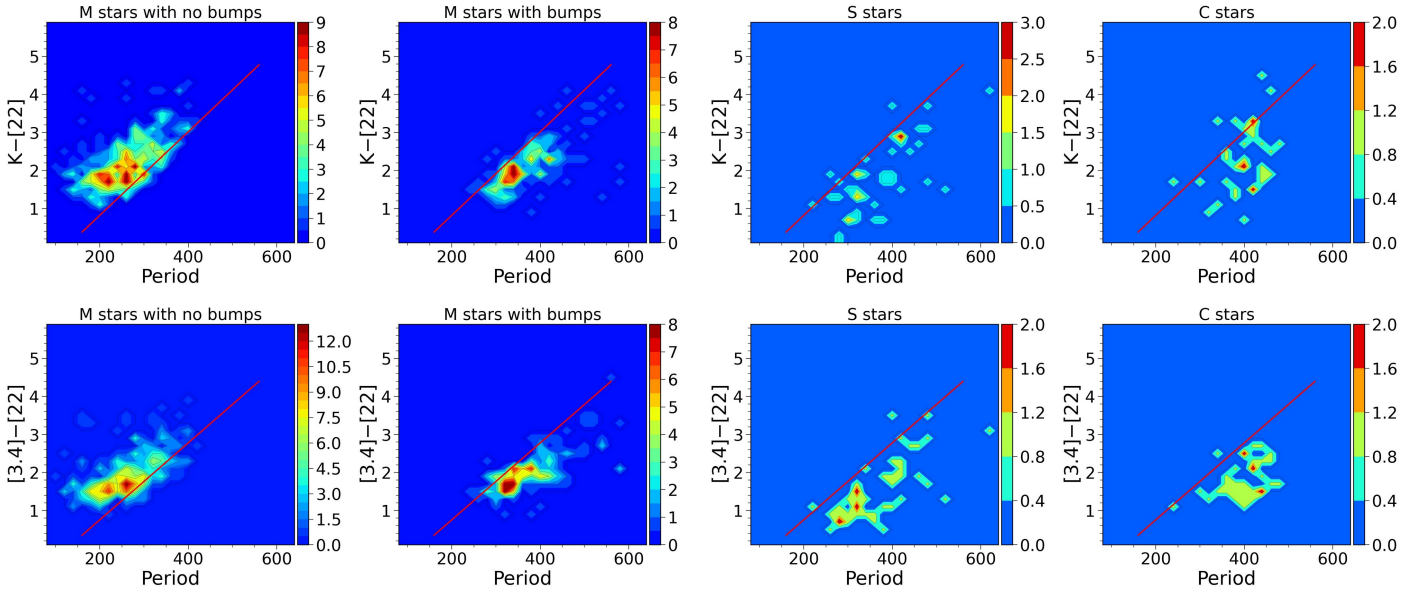


Figure 1. Distribution of the light curves of the Merchán Benítez (2023) study in the  $K-[22]$  (upper row) and  $[3.4]-[22]$  (lower row) vs period planes. The line shown in the upper row is defined by Uttenthaler et al. (2019) as  $K-[22] \sim 0.011(P-125)$ . The same line, simply scaled down using the ratio (0.92) between the mean values of  $K-[22]$  and  $[3.4]-[22]$ , is shown in the lower row.

In a preliminary phase, in order to gain some familiarity with the features displayed by different light curves, we inspected visually a sample of 35 curves of nearby stars, selected for their large apparent luminosities. It gave us the opportunity to design different forms of parameterisation and to test how they perform. We then extended such detailed inspection to four families: the 35 C-stars, the 26 S-stars, the 20 M-stars tagged as having technetium in their spectrum (referred to as Myes) and the 60 M-stars tagged as having no technetium in their spectrum (referred to as Mno) that the Merchán Benítez sample contains. This preliminary phase, about which we do not report here, has nevertheless been essential in guiding us to optimally

define how to select the samples on which the present article is based and to devise appropriate parameterisation of the light curves. After having rejected a few light curves made of observations of lesser density or quality, being particularly selective in the case of the large subsample of Mno curves, we were left with a final sample of 71 curves, referred to as sample A, containing 13 Mno stars, 14 Myes stars, 22 S stars and 22 C stars. Not included in this sample are the curves of three Mno stars, two of which display double-peak oscillations, R Cen and R Nor; the third one, X Oph, has so small oscillation amplitudes and so broad minima that it cannot be simply compared to the other curves. The clearly different nature of these three curves requires a separate analysis. Table A1 of the appendix lists the sample A curves together with information of relevance.

Many curves of sample A do not allow for a rigorous parameterisation of their shape, failing to cover a sufficient density of observations over the whole phase range, in particular around minima of luminosity. For this reason, we selected a restricted sample of 24 light curves from sample A offering a high density of observations over most of the four past decades. It includes 6 Mno, 5 Myes, 7 S and 6 C spectral types. We added to it 8 light curves of spectral type M that had been discarded from sample A because technetium had not been searched for in their spectrum or, when it had been, could not be said to be present or absent with sufficient confidence. The resulting sample of 32 light curves is referred to as sample B. Table 1 lists the values of the relevant parameters and Figure A1 of the Appendix illustrates the main results.

### 3. Defining the shapes of the selected light curves

#### 3.1 Parameterisation of the selected light curves

We start by measuring as accurately as possible the time and magnitude of each maximum and each minimum of the curve. For sample A, this can be done only approximately because of two difficulties that are met: one is the presence of flat maxima, with a very small enhancement usually located at its later edge; defining the time of the maximum as the time of the centre of the plateau or as the time of the enhancement implies differences reaching up to 8% of the period. The same difficulty is met in the analysis of Cepheid light curves, as remarked and clearly illustrated in Figure 2 of the study presented by Antonello (1993). This happens when a hump on the ascending branch reaches the maximum of the curve and eventually gets confused with it. The second difficulty relates to the evaluation of the time at minimum light and is caused by the frequent lack of observations in this low apparent luminosity region of the light curve.

For sample B, we collect the observations stored in the AAVSO database in time bins spanning typically 2% of the period. Each bin contains the number of observations, the mean magnitude and its rms value with respect to the mean. To locate the maxima, we produce a parabolic fit to these data in a time interval of 7 bins centred on the date where the maximum is expected. In the rare cases where the fit gives a date deviating by more than a bin from the centre of the interval, we may increase the size of the interval and/or iterate with an interval shifted accordingly. This procedure defines maximum dates to better than 1% of the period and maximum apparent luminosities to better than 0.1 units of magnitude. The main source of systematic uncertainty attached to the measurement of the dates is the occasional occurrence of very flat maxima.

Locating the minima proceeds similarly, except that we use broader intervals, typically of 17 bins, in order to cope with the much smaller number of observations, several bins being empty. We start with an interval centred at the phase corresponding to the mean asymmetry between ascending and descending branches and iterate the fit when necessary. We estimate that this procedure defines minimum dates to better than 2% of the period and minimum apparent luminosities to better than 0.1 units of magnitude.

Having obtained for each maximum  $i$  of the light curve a time  $T_{max,i}$  and a magnitude  $M_{max,i}$  and for its following minimum a time  $T_{min,i}$  and a magnitude  $M_{min,i}$ , we define eleven parameters as follows:

- the period  $P$ , mean value of the time separating two successive maxima,  $P = \langle T_{max,i+1} - T_{max,i} \rangle$ , and  $\Delta P$ , the rms value with respect to  $P$ , both measured in units of days.
- The mean phase of the minimum,  $\phi_{min} = \langle (T_{min,i} - T_{max,i}) / (T_{max,i+1} - T_{max,i}) \rangle$ . It is the complement to unity of the parameter  $f$  introduced by Vardya (1988) and is related to the asymmetry parameter  $\alpha = 1 - 2\phi_{min}$ .  $\Delta\phi_{min}$  is the rms value of this quantity with respect to  $\phi_{min}$ . In sample A, a direct evaluation of  $\phi_{min}$  is often not possible, because of the insufficient phase coverage near luminosity minimum. We provide instead an approximate evaluation of the asymmetry parameter  $\alpha$ , obtained from a comparison of the slopes of the ascending and

descending branches.

Table 1. Parameterisation of the 32 light curves of sample B. Columns 2 to 7 list the values taken by the parameters defined in Section 3. Columns 8, 10 and 11 are taken from Merchán Benitez et al. (2023) and list the period variation in %, the  $^{12}\text{C}/^{13}\text{C}$  ratio and the colour indices, respectively. Columns 9 and 12 list the profile type and the value taken by parameter  $K_{MB}$  as defined in Section 3.1.

<i>Mno spectral type</i>											
Name	$P/\Delta P$	$\varphi_{min}/\Delta\varphi_{min}$	$M_{max}/\Delta M_{max}$	$\Delta'M_{max}$	$A/\Delta A$	$\langle N_{dis}/Rms_{dis} \rangle$	$dP/P$	Prof.	$^{12}\text{C}/^{13}\text{C}$	dust	$K_{MB}$
R Aql	273.6/8.4	0.528/0.025	6.49/0.32	0.33	4.34/0.34	51/0.22	16.7	a	8	2.3/2.2	-0.6
R Boo	223.8/6.0	0.520/0.025	7.28/0.29	0.40	5.07/0.28	40/0.24	1.8	a	-	1.6/1.8	-0.5
R Cas	431.6/10.9	0.605/0.025	6.10/0.75	0.93	5.97/0.40	89/0.27	2.1	b	12	2.4/1.8	1.0
U Her	404.1/8.2	0.583/0.017	7.44/0.34	0.45	4.90/0.28	63/0.22	2.2	b	19	2.4/2.5	0.7
R Tri	266.0/6.0	0.522/0.022	6.24/0.32	0.46	5.35/0.29	44/0.20	1.0	a	-	1.8/1.5	-0.2
T Uma	256.1/10.2	0.583/0.030	7.77/0.53	0.70	5.28/0.33	62/0.23	2.3	a	-	2.4/2.3	-1.0
<i>Myes spectral type</i>											
R Aur	457.1/8.4	0.458/0.020	7.57/0.45	0.55	5.92/0.43	42/0.26	4.4	d	33	2.4/1.8	1.3
T Cep	338.4/13.0	0.467/0.038	6.10/0.29	0.28	4.12/0.48	117/0.23	7.0	c	33	1.2/1.2	1.7
RU Her	485.0/11.7	0.536/0.019	7.94/0.61	0.87	5.80/0.37	49/0.26	4.5	b	25	2.2/2.4	1.8
S Her	306.6/9.3	0.490/0.029	7.64/0.29	0.37	5.36/0.32	30/0.31	5.2	d	-	1.0/1.2	1.0
R Ser	354.9/9.5	0.574/0.021	6.72/0.50	0.65	6.47/0.35	69/0.23	1.7	a	14	1.9/2.0	0.6
<i>Other M spectral types</i>											
U Umi	324.3/14.9	0.502/0.043	8.29/0.28	0.20	3.26/0.37	23/0.24	3.6	d	-	1.5/1.7	0.7
V Cas	228.7/5.7	0.513/0.025	7.66/0.27	0.28	4.80/0.43	34/0.24	3.0	a	-	1.6/1.6	-0.5
T Cas	441.4/25.2	0.441/0.054	8.30/0.31	0.17	3.12/0.55	50/0.33	2.5	d	33	2.1/1.7	1.4
S Crb	360.3/11.3	0.636/0.022	7.20/0.47	0.56	5.46/0.37	65/0.22	1.9	b	-	2.7/2.8	-0.1
R Uma	300.8/6.8	0.609/0.022	7.40/0.38	0.47	5.49/0.25	78/0.23	1.7	b	-	2.9/2.8	-1.0
RT Cyg	190.3/11.1	0.536/0.027	7.38/0.45	0.62	4.65/0.32	33/0.25	1.1	a	-	1.6/1.3	-0.9
R Dra	246.8/5.5	0.546/0.022	7.60/0.42	0.49	5.13/0.27	46/0.21	2.0	a	-	2.3/1.9	-1.0
R Cvn	328.9/6.9	0.509/0.024	7.56/0.37	0.45	4.44/0.34	34/0.20	3.3	c	-	2.1/2.0	0.1
<i>S spectral type</i>											
R And	409.7/12.0	0.610/0.025	7.39/0.80	0.72	7.44/0.64	71/0.21	3.2	a	40	2.9/2.3	0.2
W And	397.5/8.8	0.575/0.021	7.92/0.68	0.90	6.29/0.31	36/0.21	1.8	b	-	1.8/1.8	1.2
R Cam	269.8/16.6	0.519/0.051	8.59/0.29	0.26	4.53/0.64	20/0.21	4.4	d	-	0.2/0.6	1.4
T Cam	375.9/15.8	0.494/0.029	8.31/0.19	0.17	5.44/0.32	23/0.20	3.8	d	31	0.8/0.5	1.9
Chi Cyg	406.9/9.2	0.549/0.018	5.14/0.68	0.91	8.31/0.37	227/0.23	2.0	c	36	2.4/1.7	0.7
R Cyg	426.7/23.1	0.619/0.026	7.90/0.83	1.45	6.15/0.25	92/0.38	2.3	a	29	2.9/2.9	0.4
S Uma	226.3/6.8	0.498/0.031	8.01/0.09	0.08	3.69/0.38	55/0.25	3.5	d	-	1.2/1.1	-0.1
<i>C spectral type</i>											
S Cam	329.0/16.4	0.478/0.041	8.59/0.12	0.11	1.84/0.21	14/0.24	2.7	d	14	0.9/1.2	1.4
W Cas	404.5/12.2	0.493/0.023	9.00/0.11	0.10	2.82/0.28	30/0.24	2.2	d/c	25	0.7/1.2	2.4
S Cep	482.6/20.7	0.460/0.026	7.97/0.44	0.41	2.38/0.20	34/0.32	3.1	c	-	2.7/1.7	1.2
V Crb	357.3/14.9	0.583/0.025	8.26/0.57	0.47	3.13/0.23	39/0.32	4.0	a	-	2.3/1.9	0.3
U Cyg	466.3/12.3	0.512/0.026	7.61/0.47	0.43	3.18/0.40	51/0.34	4.5	c	14	1.9/2.2	1.8
T Dra	423.3/16.4	0.564/0.040	9.67/0.32	0.35	3.02/0.29	16/0.33	4.0	e/a	24	3.4/2.6	-0.1

- the mean brightness at maximum light,  $M_{max}=\langle M_{max,i} \rangle$ , and its rms value with respect to the mean,  $\Delta M_{max}$ .  $M_{max}$  depends on the distance of the star to the Sun, but  $\Delta M_{max}$  provides a first measure of the global irregularity of the curve. Another, independent measure is given by the mean of the absolute value of the difference between the magnitudes of two successive maxima,  $\Delta'M_{max}=\langle |M_{max,i+1}-M_{max,i}| \rangle$ . For random magnitude fluctuations having a Gaussian distribution,  $\Delta'M_{max}=1.08\times\Delta M_{max}$ . A difference between the two parameters reveals the nature of the source of the observed magnitude fluctuations: when fluctuations between successive oscillations are small but when the magnitude of the maxima displays strong dependence on time, one expects  $\Delta M_{max}>\Delta'M_{max}$ ; if instead the magnitude of the maxima stays constant on average, but fluctuates strongly from one oscillation to the next,  $\Delta M_{max}<\Delta'M_{max}$ . There are examples of both

cases. In practice, rather than using  $\Delta M_{max}$  and  $\Delta' M_{max}$  separately, we may prefer to use their mean value,  $\Delta M_0 = \frac{1}{2}(\Delta M_{max} + \Delta' M_{max})$  and their ratio,  $R_{\Delta M} = \Delta' M_{max} / \Delta M_{max}$ .

- The mean amplitude of the oscillations, measured in units of magnitude,  $A = \langle M_{min,i} - \frac{1}{2}(M_{max,i} + M_{max,i+1}) \rangle$ ; it is sufficient to average the amplitudes of the descending and ascending branches as their means must be equal when the number of oscillations is large enough.  $\Delta A$  is the rms value of this quantity with respect to  $A$ ; it provides a third measure of the global irregularity of the curve.
- A parameter  $K_{MB}$ , referred to as the Merchán Benítez index; it makes use of the finding of Uttenthaler et al. (2019) reported in Figure 13 of the Merchán Benítez et al. (2023) article, according to which a clear separation splits the curves in two distinct families in the  $K$ -[22] vs  $P$  plane. Above a line of equation  $K$ -[22]  $\sim 0.011(P-125)$ , the curves are mostly associated with spectral type M and are smooth, at strong variance with the population below the curve. We define accordingly  $K_{MB} = 0.011(P-125) - (K-[22])$ .
- Finally, we remarked that some light curves display significantly larger dispersions than average between the magnitudes reported by different observations at a same time. At first sight, one would think that this simply reflects instrumental errors and is of no relevance to the present study. However, the effect is observed to depend on the nature of the star, being stronger for some carbon stars, which excludes an interpretation in pure terms of instrumental uncertainties. In order to study it, we select a time interval of  $\sim 6\%$  of a period, centred on each maximum and record the number of observations that it contains,  $N_{dis,i}$ , and the rms value of the measured magnitudes with respect to their mean,  $\Delta M_{dis,i}$ , and retain their mean values as two additional global parameters,  $N_{dis} = \langle N_{dis,i} \rangle$  and  $\Delta M_{dis} = \langle \Delta M_{dis,i} \rangle$ .

### 3.2 Normalised profiles

The visual inspection performed in the preliminary phase of the study had shown the difficulty to classify the light curves in terms of the lack of smoothness of the ascending branch. At first sight, many light curves appear to display regular featureless oscillations, while other display well-pronounced humps on most of the oscillations. However, a detailed inspection reveals continuity between these two groups: many curves display humps on only a small fraction of the oscillations, and the amplitude of such humps is often very small. We therefore produced for each curve of sample B a mean normalised oscillation profile, together with the distribution of the rms deviation of the individual oscillation profiles with respect to this mean profile. Normalised profiles cover from maximum  $i$  to maximum  $i+1$  and are defined as follows: the abscissa  $x$  measures the phase in 50 bins of 0.02 width, defined as 0 at  $T_{max,i}$  and 1 at  $T_{max,i+1}$ ; on the descending branch,  $x < \phi_{min,i}$ ,  $y = (M - M_{min,i}) / (M_{max,i} - M_{min,i})$  and on the ascending branch,  $x > \phi_{min,i}$ ,  $y = (M - M_{min,i}) / (M_{max,i+1} - M_{min,i})$ ,  $M$  being the mean magnitude in bin  $x$ . Like  $x$ ,  $y$  varies from 0 to 1, being equal to 0 at minimal apparent luminosity and equal to 1 at maximal apparent luminosity. In some cases, rather than normalising the oscillation profile over a whole period, we restrict it to a single branch, descending or ascending, with  $x$  spanning from 0 to 1 for  $\phi$  spanning from 0 to  $\phi_{min}$  or from  $\phi_{min}$  to 1, respectively, each time using 25 bins.

In the analysis of sample A curves, hoping to progress in the search for criteria efficient at discriminating between different light curves, we attempted at grouping them in classes associated with a specific shape of the oscillation profile. To this end, we defined five typical profile types illustrated in Figure 2. Types **a** and **e** display no hump on the ascending branch, while types **b** to **d** do. The difference between types **a** and **e** is the width of the oscillation, larger in the latter case. The hump on the rising branch is clear for type **c**, typically between phases of 5/8 and 7/8, closer to minimum for type **b** and closer to maximum for type **d**. The exercise proved to be difficult in many cases, for which the choice between two successive profiles of a pair was not obvious. This gave evidence for continuity between the sequence of profiles depicted in Figure 2, a result that may suggest that stars on the AGB would typically evolve from profile **a** to profile **e** according to such a sequence. Part of the difficulty was that a same curve often displays a broader variety of oscillation profiles than the difference between the typical profiles of the pair of candidate types. In spite of such difficulty, evidence for significant correlations between the mean oscillation profile of a curve and its spectral type was obtained. In particular, the Mno spectral type was found to be present in profile types **a** and **b** exclusively, while profile type **e** is the exclusive domain of spectral type C.

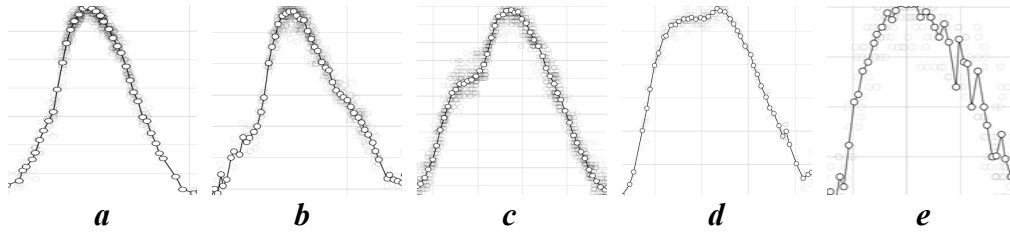


Figure 2. Typical oscillation profiles of types *a* to *e* (from left to right)

### 3.3 Humpy and hump-free families

For the light curves of sample A that are also part of sample B, we performed a 6th degree polynomial fit of the normalised profile of each oscillation of the light curves; the result is always of very good quality and we used it to define humpy curves from their behaviour in the central phases of the ascending branch, excluding the minimum and maximum regions. The match with the assignment of profile types was in general excellent.

In the case of these 24 sample B curves, with the aim to obtain a simpler and more rigorous definition of humpy and hump-free curves than obtained from the assignment of profile types *a* to *e*, we tried to distinguish them on the only basis of the mean normalised profile of the ascending branch. To the normalised profile of each branch, we fit a curve depending on a single parameter  $\lambda$ : namely, writing  $\zeta=2x-1$ ,  $\eta=2y-1$ ,

$\eta=\text{Sgn} \times \frac{1}{2} \zeta (\zeta^2 - 3) + \lambda \{1 - \zeta^2 (2 - \zeta^2)\}$  with  $\text{Sgn}=+1$  on the descending branch and  $-1$  on the ascending branch;  $\lambda$  is the value of  $\eta$  at  $\zeta=0$  ( $x=1/2$ ). They are the simplest possible polynomial forms having maxima and minima at the proper place and distorted by a single parameter,  $\lambda$ . Table 2 lists the best fit values of  $\lambda$  and  $p$ , the rms deviation between fit and data, for each branch separately and Figure 3 displays the results in the  $p$  vs  $\lambda$  plane.

They show a good match between the set of curves considered as hump-free from the assignment of profile types and the set having  $p < 0.1$  on the ascending branch, with the exception of three cases: S Her, R Cam and S Uma. These display clear humps near maximum light but their mean profiles are well described by a hump-free form having a large value of  $\lambda$ . This is better illustrated in Figure 4, which compares profiles of the four stars having  $\lambda > 0.3$  on the ascending branch (Figure 3 left), R Cam, S Uma, T Cam and S Cam. All four have a *d* type profile, the first three are of spectral type S and S Cam is of spectral type C. This illustrates the difficulty to reveal the presence of a hump when it approaches maximal luminosity, as had been remarked earlier.

A similar difficulty is met for humps near minimum luminosity. Figure 5 displays the profiles of the three curves having  $p > 0.1$  on the descending branch (Figure 3 centre), R Cas, U Her and RU Her, to which a *b* type profile had been assigned. They display clear humps on the lower part of the ascending branch but their descending branches are perfectly well-behaved. Indeed all 24 curves display a hump-free descending branch.

The risk of confusion of a hump with the minimum of luminosity is a warning that such a humpy curve may have been assigned an *a* profile type, in the same way as the S Cam curve might have been assigned an *e* profile type. In order to check on this, we display in Figure 6 the normalised profiles of the ascending branches of the nine curves retained in the hump-free family. While none of these gives evidence for the presence of a clear hump, it is difficult to reliably ascertain their absence. The right panel of Figure 3 displays the dependence of  $\lambda$  (ascending branch) on the phase  $\varphi_{min}$  at minimal luminosity. In the hump-free family, for which the fit is good and  $\lambda$  accordingly meaningful, three curves of spectral type Mno, R Aql, R Boo and R Tri, have  $\lambda$  near zero and  $\varphi_{min}$  near 0.5, implying that they are close to a sine wave. But the other six curves are slightly asymmetric, with  $\lambda$  between  $-0.24$  and  $-0.33$  and  $\varphi_{min}$  between 0.56 and 0.62. The three curves of the humpy family having  $\varphi_{min} > 0.57$  are R Cas, U Her and W And, all having profiles showing a hump on the lower part of the ascending branch. While this confirms the validity of the assignment of the curves having  $\varphi_{min} > 0.56$  to the humpy and hump-free families, respectively, it also illustrates how marginal is the distinction between these and invites prudence.

Table 2. Best fit values of the single parameter fit to the two branches of the mean normalised profiles of each of the 24



sample B light curves selected from sample A (see text).

Name	Type/ profile	Descending		Ascending		$\varphi_{min}$
		$\lambda$	$p$	$\lambda$	$p$	
Hump-free family						
R Aql	Mno/a	-0.055	0.054	-0.075	0.061	0.53
R Boo	Mno/a	-0.015	0.02	-0.065	0.031	0.52
R Tri	Mno/a	-0.075	0.046	-0.15	0.066	0.52
T Uma	Mno/a	-0.025	0.021	-0.24	0.075	0.58
R Ser	Myes/a	-0.015	0.04	-0.33	0.071	0.57
R And	S/a	0.025	0.056	-0.26	0.054	0.61
R Cyg	S/a	-0.13	0.060	-0.28	0.03	0.62
V Crb	C/a	0.005	0.031	-0.25	0.054	0.58
T Dra	C/e-a	0.035	0.039	-0.30	0.06	0.56
Humpy family						
R Cas	Mno/b	-0.065	0.11	-0.44	0.12	0.61
U Her	Mno/b	-0.16	0.11	-0.50	0.18	0.58
R Aur	Myes/d	-0.12	0.047	-0.095	0.22	0.46
T Cep	Myes/c	-0.055	0.047	0.045	0.15	0.47
RU Her	Myes/b	-0.25	0.12	-0.5	0.27	0.54
S Her	Myes/d	0.005	0.044	0.16	0.086	0.49
W And	Syes/b	0.085	0.071	-0.38	0.13	0.58
R Cam	S?/d	0.185	0.056	0.375	0.058	0.52
T Cam	Syes/d	0.175	0.057	0.495	0.12	0.49
Chi Cyg	Syes/c	-0.115	0.072	-0.22	0.11	0.55
S Uma	Syes/d	0.175	0.035	0.40	0.067	0.50
S Cam	C/d	0.28	0.044	0.40	0.078	0.48
W Cas	Cyes/d-c	0.035	0.044	0.16	0.10	0.49
S Cep	C?/c	0.055	0.037	-0.19	0.21	0.46
U Cyg	Cyes/c	0.005	0.039	-0.025	0.12	0.51

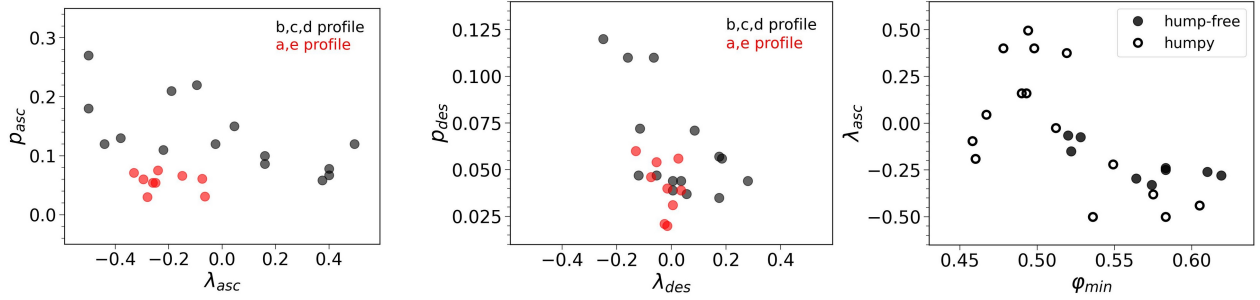


Figure 3. Dependence of  $p$  on  $\lambda$  for the ascending (left panel) and descending (central panel) branches. Black dots are for  $b$ ,  $c$  and  $d$  profiles, red dots are for  $a$  and  $e$  profiles. The right panel displays the dependence of the value of  $\lambda$  (ascending branch) on  $\varphi_{min}$ . Open circles are for the humpy family, full circles for the hump-free family.

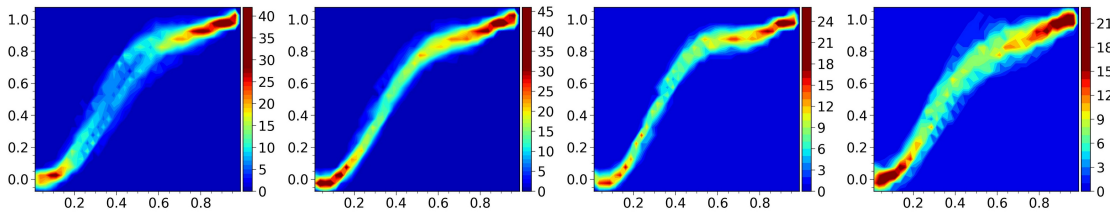


Figure 4. Superimposed normalised profiles of the ascending branch of the four curves having  $\lambda > 0.3$  on the ascending branch. From left to right: R Cam, S Uma, T Cam, S Cam.

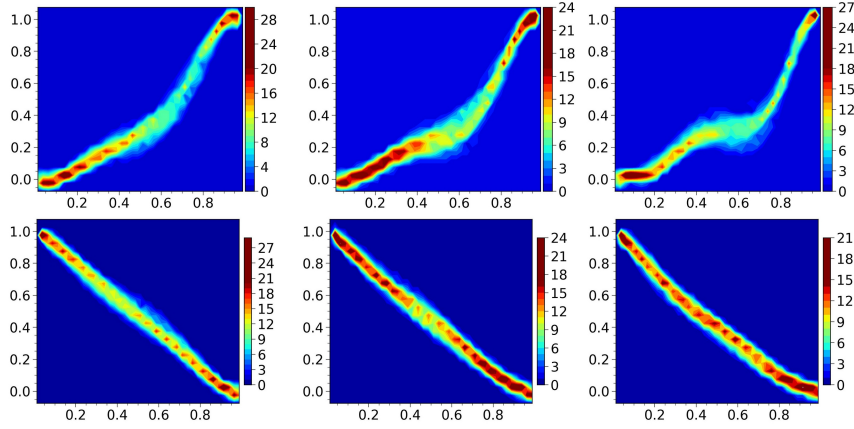


Figure 5. Superimposed normalised profiles of the ascending (upper panels) and descending (lower panels) branches of the three curves having  $p > 0.1$  on the descending branch (Figure 3 centre); from left to right: R Cas (Mno/*b*), U Her (Mno/*b*) and RU Her (Myes/*b*).

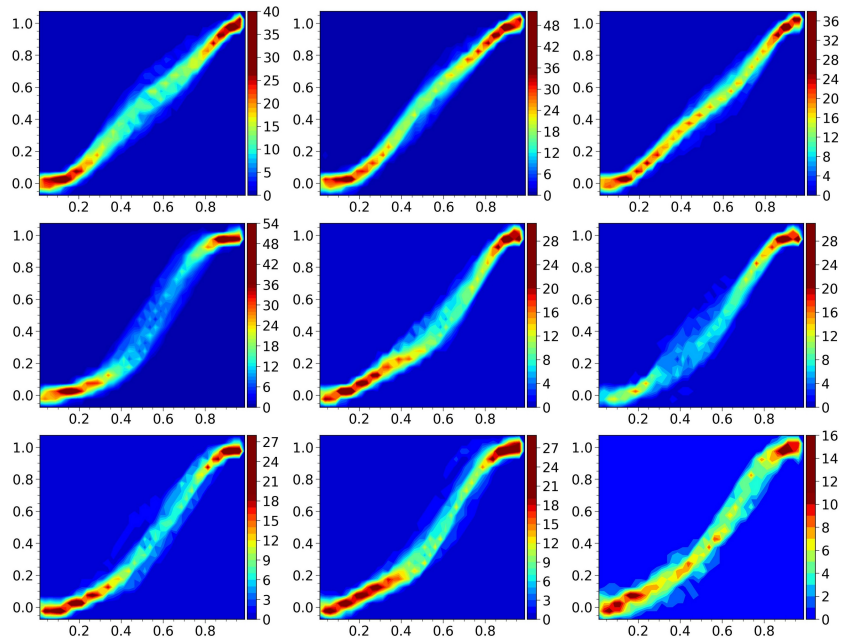


Figure 6. Superimposed normalised profiles of the ascending branches of the hump-free family. From left to right: R Aql, R Boo and R Tri (upper row), T Uma, R Ser and R And (middle row), R Cyg, V Crb and T Dra (lower row).

## 4. Oxygen-rich stars

### 4.1 Mno spectral type

In strong contrast with the other curves of sample A, which all display technetium in their spectrum when it has been searched for, the Mno spectral type family is expected to include stars that have recently entered the TP-AGB or, possibly, that are still in the E-AGB and will soon do so. Indeed, as remarked by Uttenhaler et al. (2018), it may include TP-AGB stars for which the absence of technetium in their spectrum would be caused by the first thermal pulse(s) being too weak to be followed by a third-dredge up event: only the stronger thermal pulses on the upper AGB are expected to be followed by a third-dredge-up event. It is therefore interesting to learn whether an inspection of the shapes of the light curves may help with differentiating between stars that are still on the E-AGB and stars that recently entered the TP-AGB. Also in strong contrast with the other curves of sample A, the Mno curves are exclusively made of *a* and *b* profile types. Yet, while having such strong identity, the Mno curves of sample A seem to host two different families of curves, as illustrated in Figure 7, which displays their distribution in the  $\Delta M_0$  vs  $\alpha$  and colour index vs period planes.

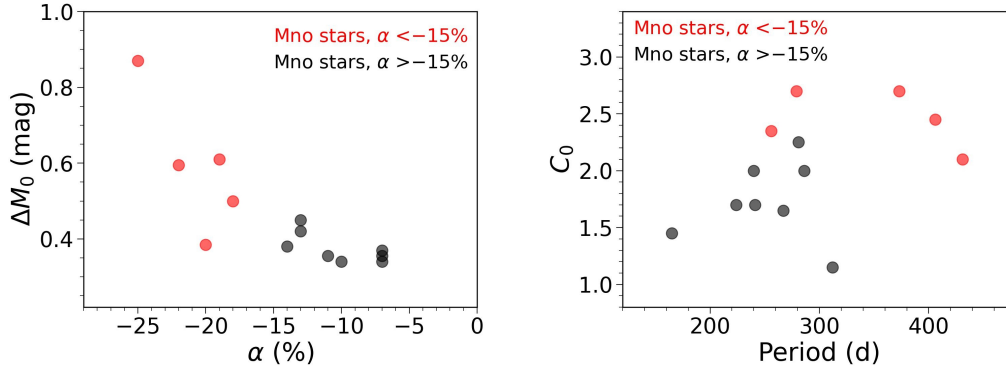


Figure 7. The Mno curves of sample A. Left: dependence of  $\Delta M_0$  on  $\alpha$ . Right: dependence of  $C_0$  on  $P$ . The red dots are for the second family.

A first nearly symmetric family, defined as having  $\alpha > -15\%$  ( $\langle \alpha \rangle = -10 \pm 3\%$ ), is relatively regular ( $\langle \Delta M \rangle = 0.34 \pm 0.04$ ,  $\langle \Delta' M \rangle = 0.41 \pm 0.04$ ), has small colour indices ( $\langle K-[22] \rangle = 1.8 \pm 0.4$ ,  $\langle [3.4]-[22] \rangle = 1.7 \pm 0.3$ ) and relatively short periods ( $\langle P \rangle = 252 \pm 42$  days). The complementary family is of course asymmetric ( $\langle \alpha \rangle = -21 \pm 2\%$ ), less regular ( $\langle \Delta M \rangle = 0.53 \pm 0.13$ ,  $\langle \Delta' M \rangle = 0.65 \pm 0.20$ ) and has larger colour indices ( $\langle K-[22] \rangle = 2.6 \pm 0.3$ ,  $\langle [3.4]-[22] \rangle = 2.3 \pm 0.2$ ) and larger periods ( $\langle P \rangle = 349 \pm 55$  days). The first family contains eight curves, generally of profile type *a*. The only exception is R Leo, of profile type *b*, with the largest period of this first family (312 days) and accordingly a positive value of  $K_{MB}$ , in contrast with the other curves of the first family, all having negative  $K_{MB}$  values. The second family contains five curves, of which three are of profile type *b* and two, W Dra and T Uma, are of profile type *a*. While the cases of R Leo and W Dra may be considered as marginal, a higher density of observations being necessary for stating with strong confidence the validity of the curve parameters, the case of T Uma deserves special attention. Its curve displays high quality and density of observations, making it belong to sample B. It has a low value of  $\alpha$  ( $-20\%$ ), or equivalently a high value of  $\phi_{min}$  (0.58), characteristic of the second family. But it has a low value of the period (256 days) characteristic of the first family. As all other parameters take values intermediate between those of the first and second family, it suggests that T Uma is in a state intermediate between the first and second family. If one assumes that Mira stars typically evolve from the first to second family, T Uma would then be currently doing so. Among the five other Mno-type curves selected in sample B, three are in the first family, R Aql, R Boo and R Tri, with respective  $K_{MB}$  values of  $-0.6$ ,  $-0.5$  and  $-0.2$ , respectively; the other two, R Cas and U Her, are in the second family with  $K_{MB}$  values of  $+1.0$  and  $+0.7$ , respectively.

These results, while broadly confirming those obtained by Merchán Benitez et al. (2023) offer a more detailed picture and imply that the line of equation  $K-[22] \sim 0.011(P-125)$  shown in Figure 1 corresponds in fact to a split between the first family of Mno-type curves, having  $K_{MB}$  negative, and the other curves.

#### 4.2 Myes and S spectral types

Figure 8 displays the distribution in the irregularity  $\Delta M_0$  vs asymmetry  $\alpha$  and colour index  $C_0$  vs period  $P$  planes of the curves of sample A having an Myes or S spectral type. All have positive  $K_{MB}$  values, in agreement with the assignments made by Merchán Benitez et al. (2023). Clear correlations are observed between the curve parameters. The more symmetric curves are also more regular and have smaller colour indices than the more asymmetric curves, which are irregular and have larger colour indices. Moreover, the more symmetric curves are exclusively of *c* and *d* profile types, while the more asymmetric are exclusively of the *a* and *b* profile types. This encourages having a global look at all sample A curves of oxygen-rich star, including the second family of Mno spectral types but excluding the first family. This is done in Figure 9, the left panel of which displays the dependence of the regularity parameters,  $\Delta M_{max}$  and  $\Delta' M_{max}$ , on the colour parameters,  $K-[22]$  and  $[3.4]-[22]$ ; the right panel displays the dependence on the asymmetry parameter  $\alpha$  of the mean colour parameter. They give clear evidence for significant correlations: more symmetric curves have smaller colour indices, probably meaning smaller dust mass-loss rate, and are more regular; more asymmetric curves, with an ascending branch

faster than the descending branch, have larger colour indices and are more irregular. However, while Mno-type curves, associated with stars that just entered the TP-AGB, are clustered in the latter group, Myes- and S-type curves populate the whole range of parameters. Moreover, the Mno-type curves are all of profile type *a*, while Myes- and S-type curves have profile types spanning from *a* to *d*. When having an *a* or *b* profile type, they tend to be on the asymmetric and irregular side, when having a *c* or *d* profile type, they tend to be on the symmetric and regular side. For stars evolving along the AGB from Mno to Myes and S types, this suggests that some of their light curves evolve all the way to a state of high symmetry and regularity with a low dust mass-loss rate while others span only a smaller path along such an evolution. In order to better understand this evolution, we study in the next sub-section how the hump, when present, evolves along the ascending branch.

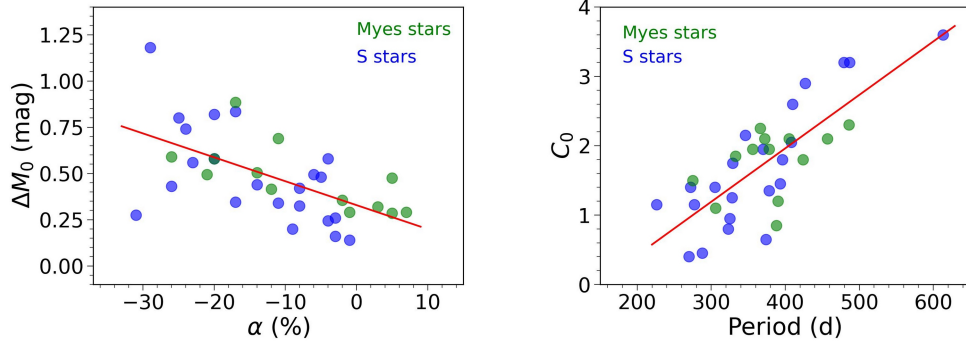


Figure 8. The Myes and S curves of sample A. Left: dependence of  $\Delta M_0$  on  $\alpha$ . Right: dependence of  $C_0$  on  $P$ . The green and blue dots are for Myes and S spectral types, respectively. The lines show linear best fits of equations  $\Delta M_0 = 0.33 - 0.013\alpha$  and  $C_0 = -1.12 + 0.0077P$ , respectively.

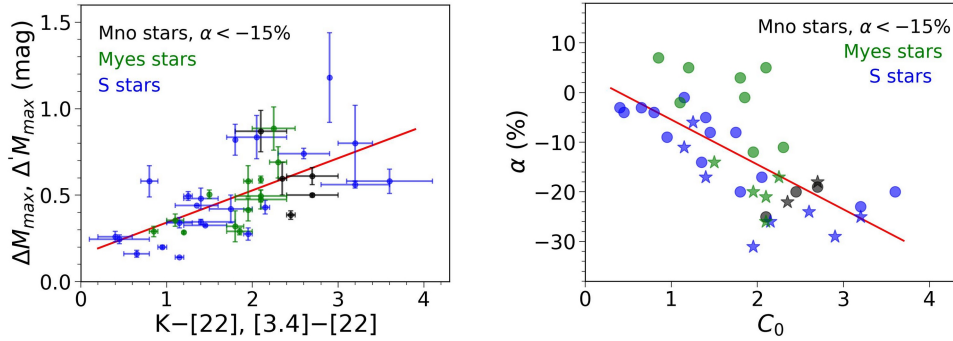


Figure 9. Curves of sample A excluding the first Mno family. Left: dependence of the regularity on colour. For each curve, we plot as ordinate a bar joining the values of  $\Delta M_{max}$  to  $\Delta' M_{max}$  and as abscissa a bar joining the values of  $K-[22]$  and  $[3.4]-[22]$ . Right: dependence of the asymmetry  $\alpha$  (percent) on the mean colour parameter,  $C_0 = \frac{1}{2}(K+[3.4]) - [22]$ . Stars are for *a* profile types. On both panels, colours correspond to spectral types as indicated in the insert and the lines are the results of linear best fits with equation  $\Delta M_0 = 0.155 + 0.186C_0$  on the left panel and  $\alpha(\%) = 3.57 - 9.03C_0$  on the right panel.

### 4.3 The hump

The evolution of type profiles for oxygen-rich stars of sample A is well illustrated by the mean values taken, for each of them separately, by the asymmetry parameter  $\alpha$ , the mean colour index,  $C_0 = \frac{1}{2}(K+[3.4]) - [22]$ , and the mean regularity parameter,  $\Delta M_0$ . They are, respectively, for the *a* profile type,  $(-20\%, 2.1, 0.58)$ , for the *b* profile type,  $(-19\%, 2.5, 0.59)$ , for the *c* profile type,  $(-3\%, 1.4, 0.45)$  and for the *d* profile type,  $(-4\%, 1.2, 0.30)$ : the *a* and *b* profiles are more asymmetric, more dusty and more irregular; the *c* and *d* profiles are more symmetric, less dusty and more regular. In order to obtain a more precise evaluation of this evolution, we use the curves of sample A that have been selected in sample B to study the evolution of the hump on the ascending branch.

We select a sample of light curves displaying a clear hump in many of their oscillations and, for each selected oscillation, fit the normalised profile of the ascending branch to a sixth-degree polynomial. The hump interval,  $[x_{hump1}, x_{hump2}]$ , is then defined as giving the best linear fit in it, the normalised magnitude spanning accordingly from  $y_{hump1}$  to  $y_{hump2}$ . The left panel of Figure 10 illustrates the procedure. The result is summarised in Table 3 and illustrated in the central panel of Figure 10. Defining  $\Delta x_{hump}$  as  $|x_{hump2} - x_{hump1}|$  and  $x_{hump}$  as  $\frac{1}{2}(x_{hump1} + x_{hump2})$  and, similarly,  $\Delta y_{hump}$  as  $|y_{hump2} - y_{hump1}|$  and  $y_{hump}$  as  $\frac{1}{2}(y_{hump1} + y_{hump2})$ , we find that the mean values of  $x_{hump}$  are poor discriminants between different curves, the rms deviations of  $x_{hump}$  with respect to the mean taking values as large as the differences between the mean values of different curves. In contrast, the central panel of Figure 10 shows that  $y_{hump}$  has rms dispersions around its mean significantly smaller than the differences between the mean values of different curves and its mean value is seen to span a broad range along the ascending branch. Typically, the rms dispersion of  $y_{hump}$  is of the order of a tenth, and  $\Delta y_{hump}$  is of the order of 14% of the oscillation amplitude. The right panel of Figure 10 displays the dependence on  $y_{hump}$  of three curve parameters: the mean colour index,  $C_0$ , the phase at minimal light,  $\phi_{min}$  and the mean irregularity,  $\Delta M_0$ .

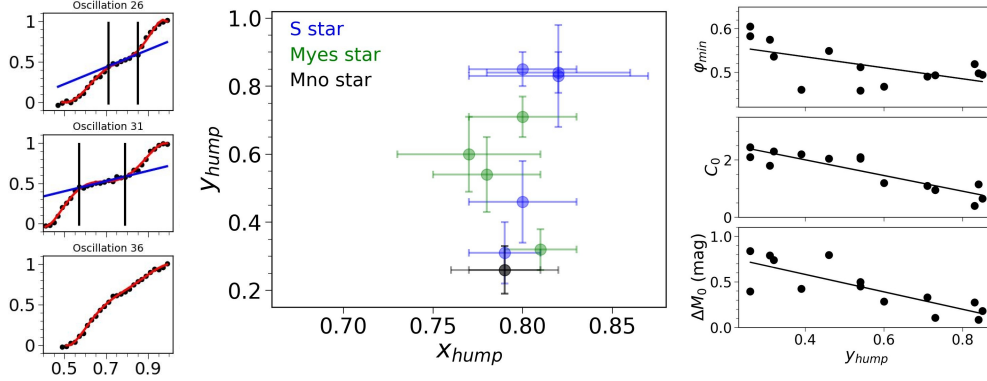


Figure 10. Left panel: illustration of the procedure used to define the hump parameters. The red curve shows the sixth-degree polynomial fit. The blue line shows the linear fit on the hump and the black lines show the hump interval. The lower panel was excluded from the sample of humpy oscillations as giving insufficient evidence for a hump. Central panel: distribution of the mean hump coordinates,  $\langle y_{hump} \rangle$  vs  $\langle x_{hump} \rangle$ , for the selected curves of sample B listed in Table 3. The error bars show the rms deviations around the mean. Right panel: dependence on  $y_{hump}$  of the parameters  $C_0$ ,  $\phi_{min}$  and  $\Delta M_0$  for the curves listed in Table 3.

#### 4.4 Recovering light curves that were ignored

In the selection of sample A light curves, M-type curves for which technetium was either not searched for or, when searched for, was found neither clearly present nor clearly absent, were deliberately ignored. Having now obtained a clearer view of the general properties displayed by the analysed light curves, we can recover such curves from the Merchán Benitez sample of 548 Mira stars, requiring that they allow for the rigorous parameterisation of the sample B selection. We select this way eight additional M-type curves: three for which technetium had not been searched for (R Uma, V Cas and U Umi), two for which the presence of technetium had been considered doubtful (R Dra and RT Cyg), two for which it had been considered possible (S Crb and R Cvn) and one for which it had been considered probable (T Cas). The curve parameters are listed in Table 1 and illustrated in Figure A1. Figure 11 below compares the 8 new M-type curves to the M-type curves belonging to both sample A and sample B. It suggests the following assignments for the new curves: V Cas, RT Cyg and R Dra, with profiles of type *a*, to the first family of Mno spectral type; S Crb and R Uma, with profiles of type *b*, to the second family of Mno spectral type; U Umi, T Cas and R Cvn, with profile types *c* and *d*, to the Myes spectral type.

Table 3. Hump parameters for curves of sample A that have been selected in sample B. The first column lists the star names, column 2 lists the spectral types, column 3 lists the profile types, column 4 lists the number of oscillations covered by the whole curve and column 5 the number of oscillations retained for the evaluation of the hump parameters, column 6 lists the mean values and rms deviations with respect to the mean of  $y_{hump}$  in percent, column 7 lists the phase at minimal light  $\varphi_{min}$ , column 8 lists the mean irregularity parameter  $\Delta M_0$  and column 9 the mean colour parameter  $C_0$ .

Name	Type	Prof	$N_{osc}$	$N_{hump}$	$y_{hump}$	$\varphi_{min}$	$\Delta M_0$	$C_0$
U Her	Mno	<i>b</i>	34	33	26/7	0.58	0.40	2.5
R Cas	Mno	<i>b</i>	33	32	26/7	0.61	0.84	2.1
S Her	Myes	<i>d</i>	44	34	71/6	0.49	0.33	1.1
RU Her	Myes	<i>b</i>	29	29	32/6	0.54	0.74	2.3
R Aur	Myes	<i>d</i>	30	30	54/11	0.46	0.50	2.1
T Cep	Myes	<i>c</i>	37	32	60/11	0.47	0.29	1.2
S Uma	S	<i>d</i>	64	54	84/6	0.50	0.09	1.2
Chi Cyg	S	<i>c</i>	35	28	46/12	0.55	0.80	2.1
T Cam	S	<i>d</i>	37	27	85/5	0.49	0.18	0.7
R Cam	S	<i>d</i>	52	42	83/15	0.52	0.28	0.4
W And	S	<i>b</i>	30	23	31/9	0.58	0.79	1.8
U Cyg	C	<i>c</i>	29	23	54/16	0.51	0.45	2.1
S Cep	C	<i>c</i>	30	30	39/14	0.46	0.43	2.2
W Cas	C	<i>d/c</i>	33	32	73/10	0.49	0.11	1.0

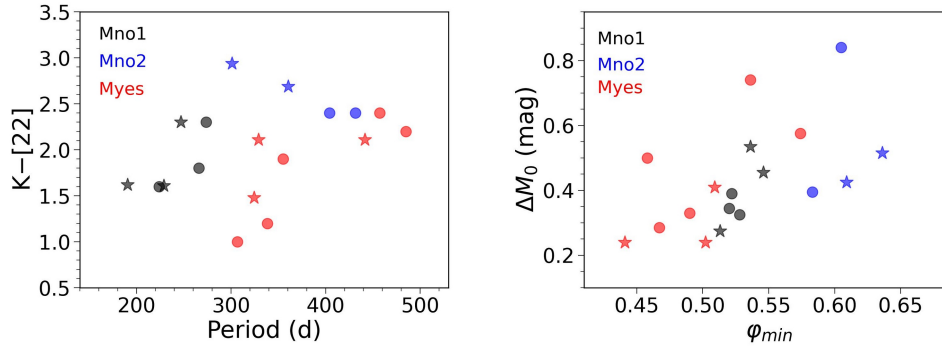


Figure 11. Comparing the M-type curves recovered in Section 4.4 (stars) to those of sample B selected from sample A (full circles). The left panel displays their distributions in the  $K-[22]$  vs  $P$  plane, the right panel in the  $\Delta M_0$  vs  $\varphi_{min}$  plane. Colours distinguish between different spectral types as indicated in the inserts. Spectral types of the eight curves recovered in Section 4.4 are as assigned in the text: V Cas, RT Cyg and R Dra to the first Mno family, S Crb and R Uma to the second Mno family and U Umi, T Cas and R Cvn to Myes.

#### 4.5 Other wavelengths

It would, of course, be important to extend the studies presented here to bandpasses other than visible, but this is a major effort beyond the scope of the present article. Unfortunately, light curves at wavelengths outside the visible bandpass are scarce and include much smaller sets of observations. Figure 12 displays the better examples of such observations for the curves of sample B. It shows, in addition to the visible B, V and R, the Johnson infrared bandpass having a mean and full width at half maximum of 806 nm and 149 nm, respectively. The main observation is that when a hump is present (absent) on the visible curve, it is also present (absent) on the infrared curve but its detailed shape may be different. This observation is consistent with the generally accepted belief that the presence of a hump is related to global properties of the star pulsation but its detailed shape is affected by the nature of the outer atmosphere. Over 50 years ago, Lockwood and Wing (1971) studied the near infrared ( $\lambda=1.04 \mu\text{m}$ ) light curves of 24 Mira variables, 15 of which are part of our sample A, and measured the ratio  $R_{IR}$  of their oscillation amplitude to that in the visible bandpass. Its mean value is 20%. It is

remarkable that the Mno curves of sample B are split in two families as clearly in terms of  $R_{IV}$  as they are in terms of  $\varphi_{min}$  and  $K_{MB}$ : R Cas and U Her have  $(R_{IV}, \varphi_{min}, K_{MB}) = (29\%, 0.61, 1.0)$  and  $(27\%, 0.58, 0.7)$ , respectively, while R Aql and R Boo have  $(R_{IV}, \varphi_{min}, K_{MB}) = (17\%, 0.53, -0.6)$  and  $(15\%, 0.52, -0.5)$ , respectively.

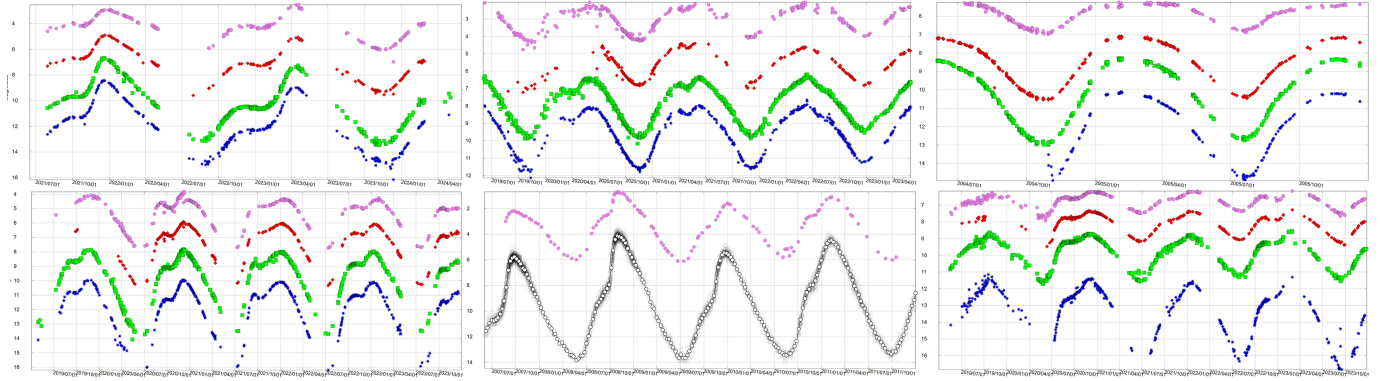


Figure 12. Intervals of the selected light curves (AAVSO data base) displaying significant observations in the B (blue), V (green), R (red) and I (magenta) band-passes. From left to right and up down, R Aur, T Cep, R Cam, T Cam, chi Cyg, W Cas.

## 5. Carbon stars

The 22 light curves of sample A carbon stars listed in Table A1 display very different features from the curves of oxygen-rich stars studied in the preceding section, the most spectacular difference being their much smaller oscillation amplitude, 2.7 mag on average compared with 5.5 mag on average for the curves of other spectral types. For many of these, the assignment as a Mira star is marginal; they are close to semi-regular variables. What makes carbon stars different from oxygen-rich stars is not the mechanism at stake inside the star, both of them burning usually hydrogen in the hydrogen-rich layer with short interruptions during which they burn helium in the helium-rich layer; this happens when the phase of hydrogen burning has produced sufficient helium ashes; it starts with violent and brief thermal pulses. What makes the difference is the composition of the star atmosphere, with dust giving it a red and sooty appearance, causing a mass-loss rate typically one order of magnitude larger than for oxygen-rich stars, a few  $10^{-6}$  rather than a few  $10^{-7}$  solar masses per year. This shortens the time left for the star to survive by making the super-wind episode come sooner. A consequence of such differences is that the evaluation of shape parameters for carbon stars is more difficult and less reliable than it is for oxygen-rich stars. Recently, significant progress has been made in both observation and modelling of the relevant mixing mechanism responsible for the S to C spectral type transition, both of which are very challenging and still suffer of several unanswered questions (Abia et al. 2022, Straniero et al. 2023).

Figure 13 displays the dependence of the irregularity  $\Delta M_0$  and asymmetry  $\alpha$  parameters on colour index  $C_0$  for the 22 curves of sample A having a C spectral type. In spite of the lesser reliability of the evaluation of the curve parameters, implying more scatter among them, the curves are seen to obey similar correlations as for oxygen-rich stars: more regular curves are also more symmetric and have smaller colour indices. However, for a same colour index, they are more regular, by typically 0.12 mag, and more symmetric, by a difference in  $\alpha$  of typically 10%, than oxygen-rich stars, possibly suggesting that once having crossed the S- to C-type boundary, the curves keep evolving a bit in such a direction.

The assignment of profile types to curves of the C family cannot be done reliably in many cases and the profiles listed in Table A1 of the Appendix are often nothing more than best guesses. It is therefore preferable to limit the study of profile types to the curves selected in sample B. These include T Dra, V Crb, S Cep, U Cyg, W Cas and S Cam and the profiles of their ascending branches are displayed in Figure 14. Remarkably, their humps cover the whole range of phases. An interpretation that may come to mind is that such stars are extrinsic carbon stars which acquired their carbon excess from a white dwarf companion long ago and are currently evolving along the AGB. In practice, however, only T Dra (Ramstedt et al. 2012) has been observed to emit X

rays, a distinctive feature of such binarity. It displays, in addition, a UV excess, as does also RU Her (Alonso-Hernández et al. 2024). But such an interpretation would not apply to the other C-stars and seems quite unlikely. Listing the values of  $(\varphi_{min}, C_0, \Delta M_0)$  for the six stars of sample B, ranked in order of increasing hump phase as shown in Figure 14, we obtain: (0.56, 3.0, 0.31), (0.58, 2.1, 0.28), (0.43, 2.2, 0.28), (0.51, 2.0, 0.37), (0.49, 1.0, 0.26) and (0.48, 1.1, 0.23), respectively. Although not perfectly, they follow the general trend that was displayed in the right panel of Figure 10 for oxygen-rich stars, giving support to the suggestion that the state of such carbon stars, the end point of their evolution on the TP-AGB, is also the end point of the evolution of their light-curves along a common path along the ascending branch, sometimes very close to its start, sometimes reaching up to its end.

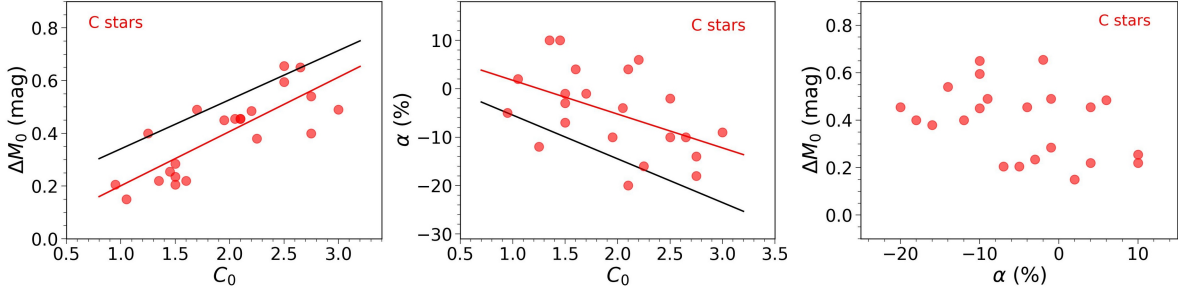


Figure 13. Sample A curves of carbon stars. Distributions of  $\Delta M_0$  vs  $C_0$  (left),  $\alpha$  vs  $C_0$  (centre) and  $\Delta M_0$  vs  $\alpha$  (right). The black lines are the best fit results to the curves of oxygen-rich stars (Figure 9), the red lines are the best fit results to the C star curves illustrated in the figure.

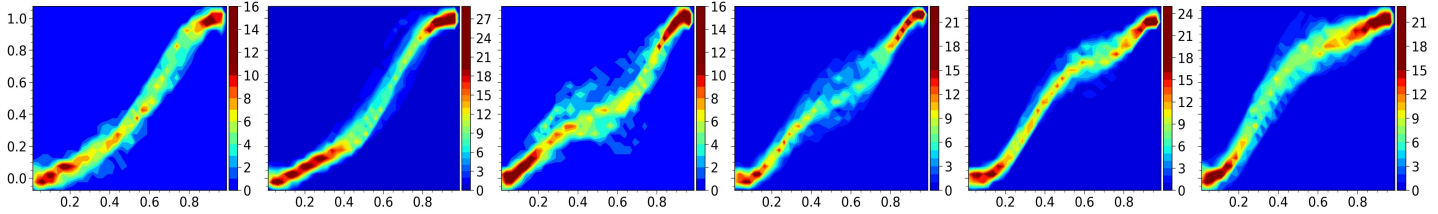


Figure 14. The ascending branches of the curves of the six carbon stars selected in sample B span the whole range of hump phases: from left to right, T Dra, V Crb, S Cep, U Cyg, W Cas and S Cam.

## 6. Regularity

The above analyses, in both Sections 4 and 5, have occasionally revealed relations between the regularity of the observed light curves, defined as the level of similarity between successive oscillations, and other parameters. We have been using two parameters to measure the regularity of the curves,  $\Delta M_{max}$  and  $\Delta' M_{max}$ . Figure 15 illustrates how the curves of sample A are distributed in the  $\Delta M_{max}$  vs  $\Delta' M_{max}$  plane. It shows that the ratio  $R_{\Delta M} = \Delta' M_{max} / \Delta M_{max}$ , which has value 1.08 in the case of random Gaussian fluctuations, is larger for the Mno spectral type and smaller for the C spectral type. This figure gives evidence for the presence of very irregular light curves, which have been accordingly excluded from sample B, but the existence of which must not be forgotten. The three worst cases, W Aql, AX Cep and R Lep have respective values of  $\Delta M_{max} / \Delta' M_{max}$  equal to 1.0/0.6, 0.8/0.5 and 0.8/0.5 and are illustrated in Figure 16. The distribution of the sample B curves in the  $\Delta M_{max}$  vs  $\Delta' M_{max}$  plane is displayed in the left panel of Figure 17. It shows the outstanding behaviour of R Cyg, with alternatively larger and smaller maxima of luminosity (Wallerstein et al. 1985, Kiss & Szatmary 2002, Roberts 2020). The right panel of the figure provides another illustration of this feature by introducing a new parameter,  $\Delta'' M_{max} = \langle |M_{max,i+2} - M_{max,i}| \rangle$ , which would be equal to  $\Delta' M_{max}$  for random fluctuations. It shows that like R Cyg, but at a much lower level, RU Her and chi Cyg display some significant correlation between the maximal luminosities of successive oscillations.

As a further illustration of the regularity of the light curves, we display in Figure 18 the dependence on the mean colour index  $C_0$ , of the dispersion at maximal luminosity,  $Rms_{dis}$ , and of the amplitude of oscillation,



A. Both show the strong homogeneity of the triplet of curves belonging to the first family of spectral type Mno. Most curves have  $Rms_{dis} < 0.3$  mag, with a mean  $\pm$  rms value of  $0.23 \pm 0.02$  mag; with  $Rms_{dis} > 0.30$  are an Myes star, S Her, and four C stars, S Cep, V Crb, U Cyg and T Dra. Together with the lower oscillation amplitude of C-type curves, the larger value of  $Rms_{dis}$  gives them often the appearance of lower quality observations. Most stars have oscillation amplitudes smaller than 7 mag, with a clear split between C-type curves,  $A < 3.5$  mag, and other spectral types,  $A > 3.5$  mag; the two curves having  $A > 7$  mag are of S-type stars R And and chi Cyg.

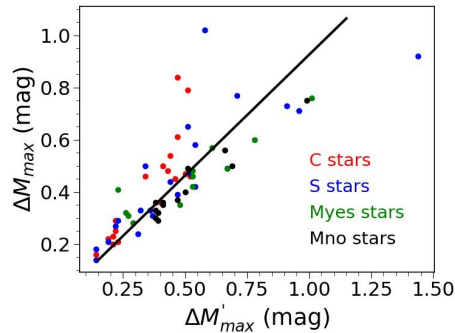


Figure 15. Distribution of the curves of sample A in the plane of irregularity parameters  $\Delta M_{max}$  vs  $\Delta' M_{max}$ . The line corresponds to the relation expected for random Gaussian fluctuations. Colours distinguish between different spectral types as indicated in the insert.

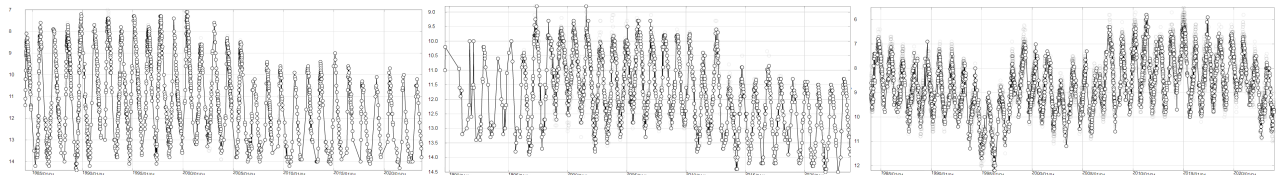


Figure 16. Irregular light curves of W Aql (left), AX Cep (centre) and R Lep (right) excluded from sample B.

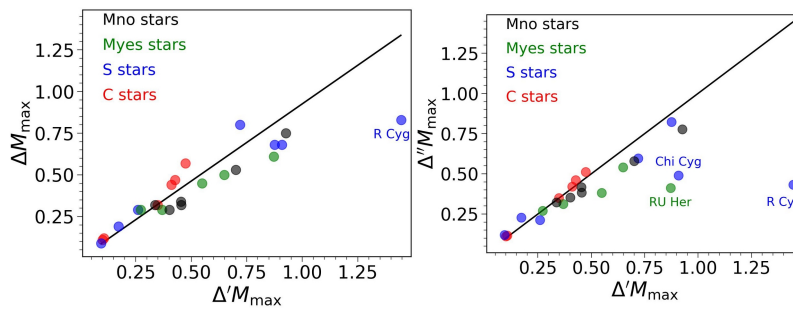


Figure 17. Distributions of the sample B curves in the  $\Delta M_{max}$  vs  $\Delta' M_{max}$  plane (left) and in the  $\Delta'' M_{max}$  vs  $\Delta' M_{max}$  plane (right).

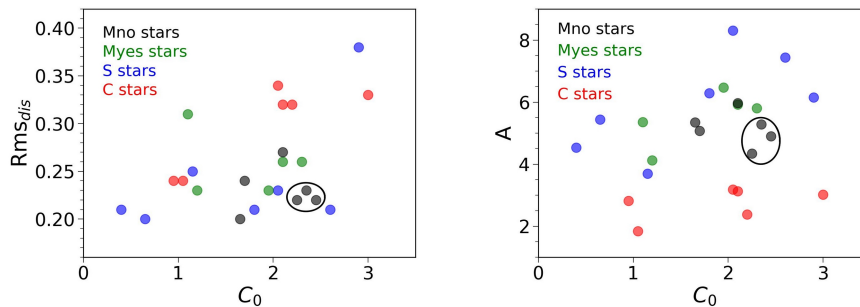


Figure 18. Distributions of the 24 sample A light curves selected in sample B in the  $Rms_{dis}$  (left) and  $A$  (right) vs  $C_0$  planes. The triplet of curves of the first Mno family is circled.

Irregularity of the periods have been abundantly studied in earlier work (Merchán Benitez et al. 2023 and references therein). In particular Zijlstra & Bedding (2002) have given evidence for three different types of period changes: continuous evolution, sudden changes and meandering periods. As mentioned in the introduction, strong period changes have been observed in a small fraction of Miras. The left panel of Figure 19 displays the distribution of the light curves of sample B in the  $\Delta P$  vs  $P$  plane, showing that most stars have  $\Delta P < 18$  days. In order to estimate how much of this is due to uncertainties in the evaluation of the time of maximal light, we show in the right panel the values taken in each curve by the mean value of the ratio  $\{P_{i+1}/\langle P \rangle - 1\} / \{P_i/\langle P \rangle - 1\}$ , the idea being that a measurement error in the time of maximal luminosity of an oscillation will increase the value of one of the adjacent periods and decrease the other. Precisely we define  $a = \langle \{P_{i+1}/\langle P \rangle - 1\} \times \{P_i/\langle P \rangle - 1\} / \{P_{i+1}/\langle P \rangle - 1\}^2 \rangle$ , which takes the value of  $-0.46$  for random measurement errors. The majority of curves have  $a$  negative as expected from the uncertainty on  $P_i$  (if  $P_i$  is measured larger than real,  $P_{i+1}$  will be measured smaller than real on average). Four curves have instead  $a$  positive, giving evidence for a systematic variability of the period: R Aur, T Cep, RU Her, all three of S spectral type, and R Aql, from the first family of Mno curves.

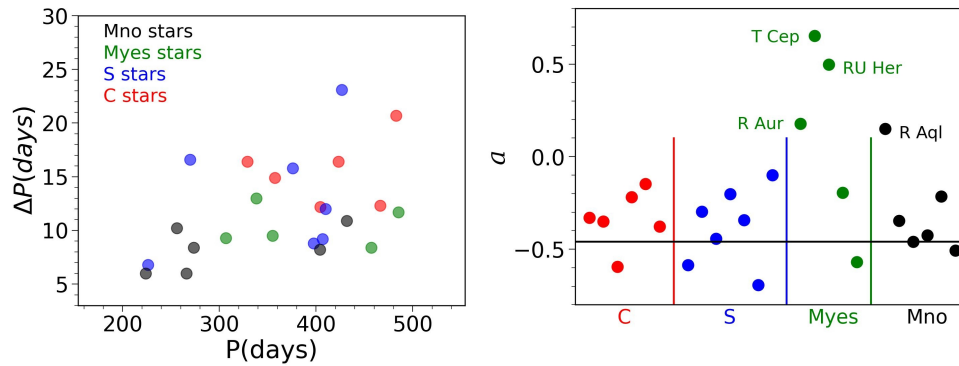


Figure 19. Regularity of the periods of the 24 sample A curves selected in sample B. Left: distribution in the  $\Delta P$  vs  $P$  plane. Right: distribution of parameter  $a$  (see text) for each spectral type separately. The horizontal line is the value expected for random measurement errors.

## 7. Discussion of the main results

The analyses presented in the preceding sections, of light curves of Mira variables selected in samples A and B, have confirmed and corroborated most of the results of earlier studies (Ludendorff 1928, Vardya 1988, Lebzelter 2011, Uttenthaler et al. 2019, Merchán Benitez et al. 2023). At the same time, they have contributed new results, the main ones being: 1) the evidence of two different families of curves of spectral type M before the occurrence of third-dredge-up events; 2) the presence of a hump on the ascending branch of many curves and its evolution; 3) the presence of correlations between the regularity, the colour index and the symmetry of the curves; 4) the uniformity of the descending branch. In the present section, we briefly summarize these results and discuss possible interpretations. We conclude with some general comments on the robustness of such new results.

### 7.1 Evidence for two distinct families of Mno type curves

The analysis of sample A curves of spectral type Mno presented in Section 4.1 has given clear evidence for a split of this group in two distinct families. Figure 20 illustrates this result for sample B. The first family is more symmetric with  $\varphi_{min}$  between 0.50 and 0.55, compared with between 0.57 and 0.65 for the second family. It has smaller periods, below 300 days, is more regular and has smaller colour indices than the second family. It is exclusively made of *a*-type profiles, while the second family contains also *b*-type profiles. It sits on the left-hand side of the colour vs period diagrams first produced by Uttenthaler et al. (2019), with  $K_{MB}$  negative, while the second family occupies also the right-hand side. When observed in infrared (Section 4.5), the ratio  $R_{IV}$  of

the infrared oscillation amplitude to that in the visible bandpass is smaller than 20% while it exceeds 25% for the second family. It includes the curves of R Aql, R Boo, R Tri, V Cas, RT Cyg, and R Dra. The second family includes the curves of R Cas, U Her, T Uma, S Crb and R Uma.

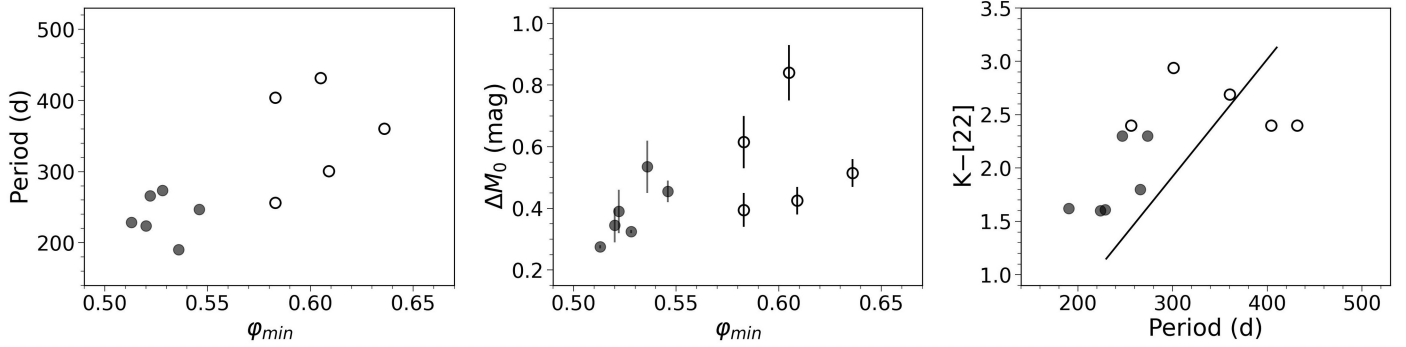


Figure 20. Sample B curves of spectral-type M identified as preceding the occurrence of third-dredge-up events. Left: period  $P$  vs phase at minimal light,  $\varphi_{min}$ . Centre: irregularity parameter  $\Delta M_0$  vs  $\varphi_{min}$ . Right: colour index  $K-[22]$  vs  $P$ ; the line is the separator defined by Utenthaler et al. (2019). Full circles are for the first family, open circles are for the second family.

All these curves have large oscillation amplitudes, on average 4.9 mag for the first family and 5.4 mag for the second family: they are clearly identified as Mira variables. When analysed in terms of Fourier series, a very powerful tool abundantly used in the published literature, they are seen to pulsate comfortably in the fundamental mode. However, for what concerns us here, Fourier series decompositions are not helpful; AGB stars are not organ pipes and what we are after is to understand the shape of a single oscillation: expressing the presence of a hump in terms of overtone contributions would not help with revealing the underlying physics. A natural interpretation of the features displayed by the curves of the first family, which are close to sine waves, is that they are associated with a well-defined phase of the evolution along the AGB, during which they are in a state that can be roughly described by only a few parameters. This would imply that the state in which a specific star is observed uniquely defines the way it will evolve and, in particular, the time when it will transition to the second family; qualitatively, this would explain why such a transition is seen as a clear separator line in two dimensional distributions of parameters defining the properties of the light curve and/or of the star itself. The transition from the first to second family would be characterised by a significant increase of the period and a slowing down of the rate of change of the size and luminosity of the star near minimal light, meaning maximal size. This may suggest that these two events are related, the slowing-down not being compensated by speeding-up during the remaining part of the period, which would then increase accordingly. The transition to the second family would also be associated with a decrease of the regularity and an increase of the colour indices, suggesting that the state of the star can no longer be defined by a very few parameters but requires a more complex description. A further advantage of such an interpretation is that it would simply explain the appearance of a hump on the ascending branch following the third-dredge-up as an evolution to larger phases of the slowing-down episode.

Such an interpretation would then imply that when transiting from the first to second family the star would experience major changes in the dynamics that govern its interior. As both the first and second families must be associated with times preceding the third-dredge-up phase, the event that could be most naturally associated with such changes is the transition from the early AGB (E-AGB) phase, during which the star is burning helium in a shell surrounding the inert core, to the thermally-pulsing (TP-AGB) phase, during which, most of the time, the star is burning hydrogen in a shell surrounding the helium shell.

To answer the questions raised by such an interpretation requires therefore a clear description of the physics phenomena underlying this transition. For a star of solar metallicity having an initial mass between 1 and 3 solar masses, the time spent on the E-AGB (from the end of helium core burning on the RGB to the first thermal pulse) is an order of magnitude larger than the time spent on the TP-AGB as oxygen-rich. Precisely, the

ratio takes values of 17, 9, 7 and 10 for initial masses of 1, 1.5, 2 and 3 solar masses, respectively (Miller Bertolami 2016). At the end of the E-AGB, the star has a small degenerated core of carbon and oxygen in its centre, surrounded by a thin helium-rich shell, itself surrounded by a thin hydrogen-rich shell, both shells being separated by a thin inter-shell layer (Herwig 2005). During the whole TP-AGB, the star is in a state fully governed by what happens in this pair of shells. What happens in the convective circumstellar envelope surrounding them and in the stellar atmosphere further out is, of course, essential to decide how the star looks like when observed from far away; but it obscures the basic dynamics causing the evolution of the star and considerably complicates the interpretation of what is observed. During the time spent on the E-AGB, the star is burning helium in the helium shell until it runs out of fuel; it keeps steadily growing in luminosity and, in the last part of the E-AGB, reaches conditions that allow it to comfortably pulsate in the fundamental mode, with radii, temperature and luminosities close to those of stars at the beginning of the TP-AGB. When running out of fuel, the star enters the TP-AGB by starting burning hydrogen around the depleted helium shell: when this will have produced enough helium ashes in the inter-shell layer, the star will experience its first thermal pulse, which will be followed by several others at intervals typically two orders of magnitude shorter than the time spent on the E-AGB. This suggests that the event marking the transition from the first to second family is the transition from the helium burning E-AGB to the hydrogen burning TP-AGB, the former curves being associated with Mira stars at the very end of the E-AGB.

## 7.2 Presence of a hump on the ascending branch of some light curves

In Section 4.2, to each curve of oxygen-rich stars selected in sample A, we have assigned a profile type, ranking from *a* to *d*, the three latter displaying a hump on the ascending branch at increasing phases. We noted that the curves having oscillations of *a* and *b* profile types are more asymmetric, more dusty and more irregular; those having oscillations of *c* and *d* profile types are more symmetric, less dusty and more regular. In Section 4.3 we studied curves of sample B displaying a clear hump and we evaluated its magnitude, normalised to the oscillation amplitude,  $y_{hump}$ . We found that its rms dispersion with respect to its mean is of the order of a tenth, and that the width of the hump is of the order of 14% of the oscillation amplitude. On average (Figure 10 right), we have shown that the parameters  $\varphi_{min}$ ,  $C_0$  and  $\Delta M_0$  are decreasing functions of  $y_{hump}$ .

This might have suggested that when entering the third-dredge-up phase of the TP-AGB, the curves develop a hump, first confused with the luminosity minimum and then progressively climbing the ascending branch up to maximal luminosity. Such a suggestion could even have been extended to carbon stars such as S Cam. But this is not what happens. While curves of increasing spectral type, from M to C, may indeed reach up to increasingly larger values of  $y_{hump}$ , each spectral type is seen to cover the whole corresponding  $y_{hump}$  range rather than clustering at its end. This is illustrated in Table 4, which lists, for each spectral type and each profile type separately, the number of curves selected in samples A and B. We recall that the assignment of type profiles is less reliable for sample A than for sample B, which, however, includes only half as many curves. But the assignments made in sample B can be trusted as reliable and their diversity was clearly illustrated in Figure 14 in the case of carbon stars. It looks like if, when progressing along the TP-AGB from M to C spectral types, the star experiences something that causes a slowing-down episode of the pulsation when it is on the ascending branch of the light curve. The phase at which this happens would start at minimal light and would increase together with the C/O ratio that measures the progression of the star on the TP-AGB. However, this phase would stop increasing at some point, the star continuing its evolution along the TP-AGB while the slowing-down episode persists but stays at a fixed phase. This is of course pure speculation; what we observe is intriguing and challenges interpretation.

Such humps are also observed on the light curves of other pulsating stars. In the case of RR Lyrae (Prudil et al. 2020 and references therein) they track shock waves caused by a rapid compression of the star atmosphere: they are the result of a sudden stop of the infalling photosphere and immediate outward expansion. Kudashkina and Rudnitskij (1994) have remarked that a similar mechanism could be at stake in the case of Mira stars. Using a simple model of the propagation of shock waves in the star atmosphere, heating the gas to temperatures sufficient for ionisation, they show that the duration of the resulting hump is of the order of a tenth of a period, in good agreement with observations. In the case of Cepheids (Bono et al. 2000, Marconi et al. 2022

and references therein) the hump is on the ascending branch for periods larger than  $\sim 11$  days and on the descending branch otherwise (the so-called Hertzsprung progression, Hertzsprung 1926). State-of-the-art non-linear convective pulsation models, accounting for the movement of pressure waves in the star interior including reflections and resonances, provide descriptions of the Hertzsprung progression in good agreement with observations (Marconi et al. 2022).

However, in the case of Mira light curves, and in spite of numerous and detailed descriptions that have been available for decades (Schorr 2016 and references therein, Templeton 2005, Marsakova & Andronov 2007, Lebzelter 2011, Merchán Benitez et al. 2023), we lack a reliable interpretation of what is causing them. The suggestion (e.g. Lebzelter 2011) that they may simply result from a resonance between the fundamental and the first overtone modes seems unlikely, the light curves of Mira stars having large oscillation amplitudes implying that the stars are in conditions allowing them to comfortably pulsate in the fundamental mode. Merchán Benitez et al. (2023) suggest instead that dust being formed inefficiently in the wake of an outwardly propagating shock wave would fall back toward the star instead of being accelerated outwards and would hit the outwardly moving shock wave of the next pulsation cycle, thereby causing humps or secondary maxima in the light curve.

Table 4. Number of light curves selected in samples A and B, listed according to their spectral type and profile type, separately. Five sample A curves have been excluded as having a too poorly defined profile type.

	Sample A (66 curves)					Sample B (32 curves)				
	<i>a</i>	<i>b</i>	<i>c</i>	<i>d</i>	<i>e</i>	<i>a</i>	<i>b</i>	<i>c</i>	<i>d</i>	<i>e</i>
<i>Mno1</i>	6	1				6				
<i>Mno2</i>	3	3				1	4			
<i>Myes</i>	5	2	3	3		1	1	2	4	
<i>S</i>	8	3	4	7		2	1	1	3	
<i>C</i>	6	0	5	3	4	1	0	2	2	1

### 7.3 Presence of correlations between regularity, colour index and symmetry of the curves

Figure 9 has given evidence for significant correlations between the parameters describing the sample A light curves of oxygen-rich stars, spectral-types M to S. The more symmetric curves, exclusively made of *c* and *d* profile types, were observed to be more regular and have smaller colour indices than the more asymmetric curves, exclusively made of *a* and *b* profile types, which are irregular and have larger colour indices. Figure 13 has shown that a similar trend is followed by the curves of carbon stars, which, however, for a same colour index, are more regular and more symmetric than the curves of oxygen-rich stars. Figure 21 displays the dependence on colour index,  $C_0$ , of the regularity parameters,  $\Delta M_{max}$  and  $\Delta'M_{max}$  (left) and of the phase at minimal light,  $\varphi_{min}$  (right) for the curves of sample B. It qualitatively confirms the general trend found for sample A: the average slopes for sample A (Figure 9) were 0.19 mag of  $\Delta M_0$  and 4.5% of  $\varphi_{min}$  per unit of magnitude of the mean colour index  $C_0$ . They are now, for sample B, 0.23 mag of  $\Delta M_0$  and 5.4% of  $\varphi_{min}$ .

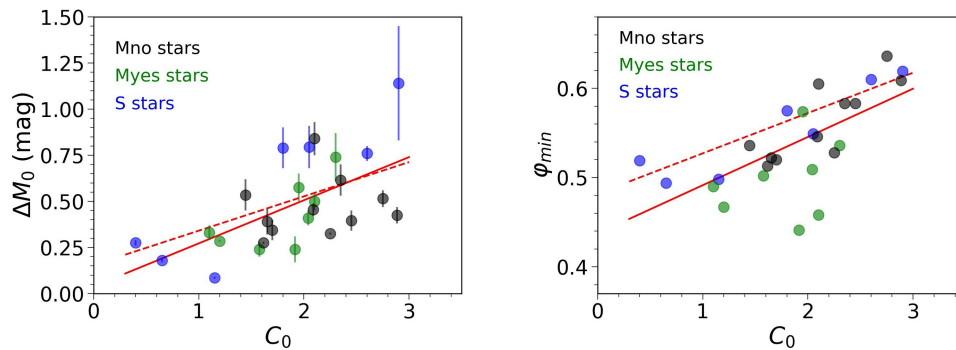


Figure 21. Sample B curves. Dependence on colour index  $C_0$  of the regularity parameters  $\Delta M_{max}$  and  $\Delta'M_{max}$  and of the phase at minimal light,  $\varphi_{min}$ . A bar joins the values taken by  $\Delta M_{max}$  and  $\Delta'M_{max}$  at a same value of  $C_0$ . Different spectral-types are shown with different colours as shown in the inserts. The full red lines show linear fits to  $\Delta M_0 = \frac{1}{2}(\Delta'M_{max} + \Delta M_{max})$  and to  $\varphi_{min}$  and the dashed red lines show the same linear fits obtained for sample A (Figure 9).

While reliable and robust, the above result is only valid on average and the curve parameters shown in Figure 21 display major dispersion with respect to the mean. This can be understood in part as an effect of the thermal pulses that occur at a typical rate of one every  $10^5$  years (Miller Bertolami 2015, Marigo et al. 2013). While very short, only a few years, these pulses are so violent, with temperatures up to a few  $10^8$  K, that they can be expected to disturb the interior and the atmosphere of the star for a significant fraction of the inter-pulse phase. In particular, this argument has been used by Merchán Benitez et al. (2023) to explain the occasional observation of period changes, the more drastic the closer to the thermal pulse. Some parameters, such as the C/O ratio, the amount of technetium in the spectrum, the  $^{12}\text{C}/^{13}\text{C}$  ratio, increase progressively after each third dredge-up episode and are not expected to display significant scatter. But others, such as temperature and turbulence, can be expected to be deeply affected, causing major temporary changes in the pulsation regime. However, such an interpretation seems unlikely to apply to the near totality of the curves illustrated in Figure 21. Such major scatter must be seen in the context of other puzzling features that Mira stars light curves display over the TP-AGB phase, such as major changes that affect their shape from one oscillation to the next, as discussed in Section 6; these include, in particular, the value of  $y_{\text{hump}}$  and the intensity with which a hump may occur, but also, to a lesser extent, the maximal luminosity and the period. Another puzzling feature worth mentioning in this context is the absence of S- and C-types meandering period changes (Merchán Benitez et al. 2023). Also of relevance is the possibility for the curve of a given star to stop being of the Mira pulsation type, either momentarily or definitively. This may happen on the occasion of thermal pulses but may also happen in other occasions. In particular, we noted that many of the sample A curves of carbon stars are closer to the semi-regular type of pulsation than to the Mira type.

What makes it difficult to devise sensible interpretations of observations that must necessarily be made from outside the star, is that its appearance is the consequence of a long chain of causally connected events: it starts from nuclear burning around the inert core, continues with the properties of the convective zone and ends with the inner and outer atmospheres of the star. Ideally, one would like to understand nuclear burning and convection before having to deal with the complexity of the nascent wind, dust formation and radiation pressure. In this context, the latter, not to mention the impact of a possible companion, seem unfortunate complications that prevent a clear identification and description of the more basic mechanism at stake inside the star. In particular, quantities such as the mass loss rate (Uttenthaler et al. 2024 and references therein) or the  $^{12}\text{C}/^{13}\text{C}$  isotopic ratio are known to be both episodic and anisotropic: their properties are very complex and their evaluation requires a detailed understanding of the radiative transfer taking place in the atmosphere, of the shock chemistry of relevance and of the dust formation process (e.g. Darriulat et al. 2024, Hoai et al. 2024). As a result, very large uncertainties are attached to such quantities: apart from general trends, well documented in the published literature, they seem unlikely to help significantly with the understanding of the features addressed in the present article. Yet, while strongly affected by the properties of the star atmosphere, light curves are also apt at revealing features taking place inside the star, which makes a detailed study of their shapes particularly valuable.

#### 7.4 Uniformity of the descending branch

In Section 3.3, we briefly commented that all curves of sample B display a hump-free and smooth normalised profile of the descending branch. This is important information, worth additional comments. Even if we know of a few, extremely rare cases of oscillations that seem to display a small hump on the descending branch, we can consider this as a robust and reliable result. The left pair of panels of Figure 22 compares the superimposed normalised profiles of all oscillations of the ascending branches of the sample B curves with those of the descending branches. Curves of the first Mno family are shown separately from the other 24 curves. The figure offers a spectacular illustration of the difference between the ascending branches of these 24 curves and either their descending branches or both the ascending and descending branches of the first Mno family. In order to better quantify such a result, we fit each normalised profile of the ascending and descending branches observed in the oscillations of the 32 light curves of sample B with the form defined in Section 3.3; it uses a single

parameter  $\lambda$  that measures, for each branch separately, the deviation from mean magnitude ( $y=1/2$ ) at mean phase ( $x=1/2$ ). The distributions of the number of profiles as a function of  $\lambda$  are displayed in the right panels of Figure 22. The mean/rms values of  $\lambda$  are  $-0.01/0.16$  for the descending branches of the first Mno family,  $-0.07/0.17$  for its ascending branches and  $-0.01/0.17$  for the descending branches of the 24 other curves. Of course, the similarity revealed by comparing these three distributions does not mean that all curves share a same branch profile. They span different fractions of the period, measured by the different values taken by  $\varphi_{min}$ , and different fractions of the oscillation amplitude. But it means that no special event seems to take place when the luminosity of the star decreases, nor when it increases in the case of the first Mno family. This is at strong variance with the clear evidence for something specific happening, taking the form of a slowing-down episode, when the luminosity increases, in the 24 other curves. It provides another illustration of the results presented in sub-sections 7.1 and 7.2.

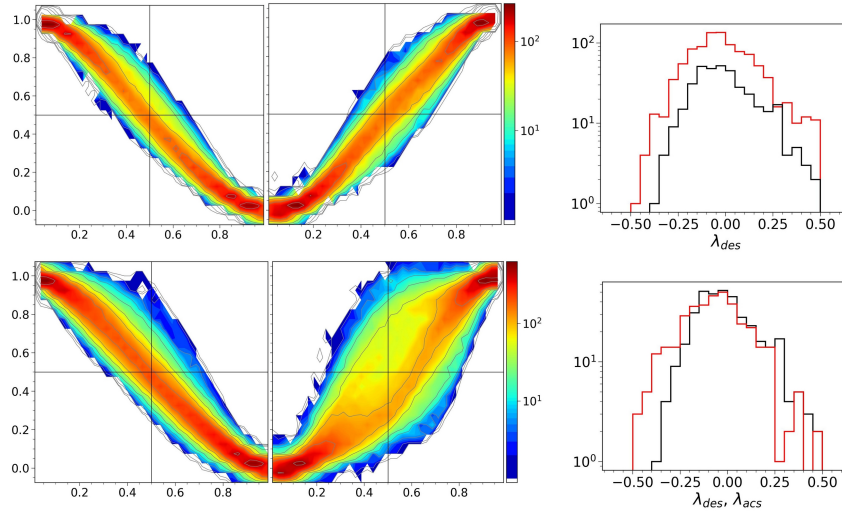


Figure 22. Left pair of panels: superimposed normalised profiles of the descending and ascending branches of sample B curves. The 8 curves of the first Mno family ( $\sim 370$  oscillations) are displayed on the upper row and the 24 other curves ( $\sim 1000$  oscillations) are displayed on the lower row. The colour scales are logarithmic. Right panels: distribution of the parameter  $\lambda$  (see text) comparing the descending branches of the Mno1 family (red) with the descending branches of the other curves (black, upper row) and with the ascending branches of the Mno1 family (black, lower row).

### 7.5 Peculiarities

The results obtained in the present article deliberately ignored peculiarities that might have distracted us from trying to reveal general features. Yet several such peculiarities have been met and, while it is beyond the scope of the present article to address them, we know that science often progresses by detailed scrutiny of anomalous cases and we briefly list the main ones in the present sub-section.

X Oph is an Mno curve but shares none of the properties displayed by pre-third-dredge-up curves: it has  $P=334$  days compared with a mean of 244 days,  $\Delta M_0=0.25$  mag compared with 0.41 mag,  $R_{AM}=1.0$  compared with 1.2,  $A=1.7$  mag compared with 5.1 mag,  $K_{MB}=0.2$  compared with  $-0.7$ ,  $W_{1/2}=0.29$  compared with 0.46,  $\alpha=-2\%$  compared with  $-12\%$ .

R Cen and R Nor are also Mno curves, with respective periods of 572 and 498 days, but they display a double-peaked oscillation profile. It has been recurrently argued in the literature that the periods are in fact half these values and that oscillations of higher and lower apparent luminosity alternate (Templeton & Willson, no date). Hawkins et al. (2001) argue that R Cen is probably experiencing a helium-shell flash and that the most likely cause of double-peaking is a resonance between two modes, but Garcia-Hernandez et al. (2013) show instead that R Cen is a massive hot-bottom-burning AGB star. One often reads in the published literature that “*R Cen used to have an unusual double-peaked light curve, but by 2001 this had reverted to an almost normal single-peaked curve*”, but this statement is incorrect. From a study of lithium in the spectra of R Cen and R Nor, Uttenthaler et al. (2012) suggest that both are undergoing the hot-bottom-burning phase.

R Aql was found in Section 6 (Figure 19 right) to show evidence for a systematic variability of its period, which is indeed known to have declined from 320 days in 1915 to 264 days in 2010 (Zhao-Geisler et al. 2012). This is surprising for a star of spectral type M that displays no technetium in its spectrum, has a low  $^{12}\text{C}/^{13}\text{C}$  ratio of only 8, and has been identified in the present work as a clear candidate of the first Mno family. Wood & Zarro (1981) have shown that such a period change could very well be interpreted as the consequence of a recent thermal pulse, in which case the curve would belong to the second, rather than first, Mno family.

R Gem, an S curve with a clear *a*-type oscillation profile, stands out as being quite regular ( $\Delta M_{\sigma}=0.27$  mag,  $R_{\Delta M}=1.3$ ) together with a very large asymmetry ( $\alpha\sim 30\%$ ), two properties that usually do not go together. It has a  $K_{MB}$  value of 0.8. As it has a period very close to a year (370 days) it suffers from being always observed at the same phase from a given longitude, but this does not explain its peculiarity.

R Cyg, another S curve, shows spectacular episodes of alternating maxima of luminosity, that were discussed in Section 6 together with other extreme cases of irregularity including R Lep, R Cas and W Aql. Extreme values of the period include: below 200 days, T Her (165 days) and above 500 days, R Cen (572 days), BH Cru (529 days) and S Cas (613 days). R Lep is a carbon rich star which has been the target of many observations (Rau et al. 2017, Asaki et al. 2023, and references therein). W Aql is an S-type star, which has also been abundantly observed (Danilovich et al. 2014, Brunner et al. 2018); De Beck and Olofsson (2020), from a study of the chemistry of the gaseous component of its CSE, have concluded that it appears considerably closer to a C-type star than to an S-type star. Mayer et al. (2013) have detected a companion at a separation of 160 au. BH Cru is known for the high variability of its period (Loidl et al. 2001). Zijlstra et al. (2004), from a study of its evolution, argued that it is unlikely to be related to an ongoing thermal pulse. Walker (2009) studied changes in the light curve and Uttenthaler et al. (2011) discussed the period changes and the transition from spectral type S to C. S Cas has been observed to have a high mass loss rate, of  $\sim 1.8 \cdot 10^{-6}$  solar masses per year, by McDonald et al. (2018). The pulsation period of R Hya has been observed to decline and Uttenthaler & Lebzelter (2010), from a study of technetium and lithium in its spectrum, have argued that, while this decline may be related to a recent thermal pulse, such pulses would not be strong enough to generate a third dredge-up. The CSE has been a target for numerous observations (Homan et al. 2021, Joyce et al. 2024, and references therein).

## 8. Summing up

In the present work, we have selected visual curves of Mira variables that offer sufficient density and quality of observations for a reliable parameterisation of their shape. Depending on how severe the selection was, it produced a sample A of 71 curves or a sample B of 32 curves. While having corroborated most of the results of earlier studies, our work contributes new significant results: 1) the evidence for the presence of two distinct families of curves of spectral type M before the occurrence of third-dredge-up events, suggesting that they make a distinction between stars at the end of the E-AGB and stars at the beginning of the TP-AGB. 2) The presence of a hump on the ascending branch of many curves, suggesting that it is associated with a slowing-down of the rate of luminosity increase on the ascending branch that is climbing it as the star evolves along the TP-AGB, being seen as a broadening of the minimum when it starts deviating from it and as a broadening of the maximum if and when it reaches it. 3) The presence of correlations between the regularity, the colour index and the symmetry of the curves; while the evidence for their existence as a general average trend is a robust and reliable result, a very large scatter of the curve parameters with respect to such average significantly weakens the relevance of these correlations and challenges a reliable interpretation. 4) The uniformity of the descending branch has been clearly demonstrated and shown to give evidence for the absence of specific event occurring on its phase of the pulsation.

A sensible explanation of these results is still lacking. They suggest the existence of a slowing-down episode of the pulsation mechanism associated with an increase of the pulsation period; it happens when the star enters the TP-AGB phase, namely is absent when the star burns helium around the core and present only when it burns hydrogen around the helium shell. Moreover this slowing-down episode is related to the details of the kappa-mechanism that governs the pulsation, being observed exclusively on the ascending branch of the light curve, and being seen to evolve along this branch in correlation with the time spent by the star on the TP-AGB. Understanding what is going on requires therefore understanding both the nuclear processes at stake, in



particular which difference between helium burning and hydrogen burning has an impact on the dynamics of the kappa-mechanism, and understanding the details of the kappa mechanism itself, in particular concerning convection, shock waves and the morphology of the ionisation zone. A speculative interpretation would imply that some new feature appears at the transition between the helium-burning E-AGB and the hydrogen-burning TP-AGB. It might, for instance, take the form of a shock wave that would repeat at each oscillation of the hydrogen-burning inter-pulses of the TP-AGB and would ionise part of the envelope as first suggested by Kudashkina & Rudnitskij (1994).

The complexity and diversity of the light curves, the strong variability that they display from one oscillation to the next, and the absorption caused by the dust-rich outer atmosphere, make it particularly difficult to provide reliable interpretations, in particular to make a clear distinction between events occurring inside the star and events occurring in its atmosphere. Our approach has been to reveal general trends at the price of ignoring apparent anomalies. One must not underestimate the speculative character of many of the conclusions that we have been proposing. As we are unable to state reliable interpretations with sufficient confidence our aim has more modestly been to trigger reactions and inspire new studies that would either confirm or deny our findings. Yet, the rich set of results that we have been able to obtain confirms our feeling that the outstanding set of high-quality observations of visual light curves of LPV AGB stars has not yet been exploited as thoroughly as it deserves.

## Acknowledgements

To the extent that the analyses presented in the present article may have contributed some progress, the credit belongs to the innumerable observers around the world and to the AAVSO, without whom none of the results could have been obtained. We are accordingly deeply indebted to them: to the many observers for the high quality of their observations and to the AAVSO for the outstanding handling and reduction of the data that makes their use particularly easy and efficient.

We are deeply grateful to Professor Stefan Uttenthaler, who published, together with colleagues, several seminal articles that largely inspired our work, for having patiently listened to and answered our many questions. We thank him deeply for having shared with us his views and understanding of many of the issues at stake in the present work.

Financial support from the World Laboratory, the Rencontres du Vietnam, the Vingroup Innovation Foundation under project code VINIF.2023.DA.057 and the Vietnam National Space Center is gratefully acknowledged.

## References

- Abia, C., & Isern, J., 1997, *Carbon ( $^{12}\text{C}/^{13}\text{C}$ ) and Oxygen ( $^{16}\text{O}/^{17}\text{O}$ ) Isotopic Ratios in Seven Evolved Stars*, MNRAS, 289, L11
- Abia, C., de Laverny, P., Romero, M. & Figueras, F., 2022, *Characterisation of Galactic carbon stars and related stars from Gaia EDR3*, A&A, 664, A45
- Alonso-Hernández, J., Sánchez Contreras, C. & Sahai, R., 2024, *CO emission survey of asymptotic giant branch stars with ultraviolet excesses*, A&A, 684, A77
- Andrassy, R., Higl, J., Mao, H. et al., 2022, *Dynamics in a stellar convective layer and at its boundary: Comparison of five 3D hydrodynamics codes*, A&A, 659, A193
- Andrievsky, S.M., Luck, R.E., & Kovtyukh, V.V., 2005, *Phase-dependent Variation of the Fundamental Parameters of Cepheids. III. Periods between 3 and 6 Days*, AJ, 130, 1880
- Antonello, E., 1993, *The asymmetry parameter  $M-m$  of the light curves of Cepheids in the Galaxy and Magellanic Clouds*, A&A, 279, 125
- Asaki, Y., Maud, L.T., Francke, H. et al., 2023, *ALMA High-frequency Long Baseline Campaign in 2021: Highest Angular Resolution Submillimeter Wave Images for the Carbon-rich Star R Lep*, ApJ, 958, 86
- Bono, G., Marconi, M. & Stellingwerf, R.F., 2000, *Classical Cepheid pulsation models VI. The Hertzsprung progression*, A&A, 360, 245
- Bowers, P.F., 1975, *On the Light Curves of OH-Mira Variables*, A&A 39, 473

- Bowers, P.F. & Kerr, F.J., 1977, *OH Mira variables - the light curve shapes and implications for mass loss*, A&A 57, 115
- Brunner, M., Danilovich, T., Ramstedt, S., 2018, *Molecular line study of the S-type AGB star W Aquilae*, A&A, 617, A23
- Danilovich, T., Bergman, P., Justtanont, K., 2014, *Detailed modelling of the circumstellar molecular line emission of the S-type AGB star W Aquilae*, A&A, 569, A7
- Darriulat, P., Hoai, D.T., Nhung, P.T. et al., 2024, *On the nascent wind of oxygen-rich AGB stars: scrutiny of a sample of nearby stars*, Comptes Rendus de l'Académie des Sciences, 25, 219-250
- De Beck, E. & Olofsson, H., 2020, *The surprisingly carbon-rich environment of the S-type star W Aql*, A&A, 642, A20
- Eddington, A.S., 1917, *The pulsation theory of Cepheid variables*, The Observatory, 40, 290
- Freytag, B. & Höfner, S., 2023, “*Global 3D radiation-hydrodynamical models of AGB stars with dust-driven winds*”, A&A, 669, A155
- Gal, J., & Szatmary, K., 1995, *T Ursae Minoris: a Mira star with rapidly decreasing period*, A&A, 297, 461
- García-Hernández, D.A., Zamora, O., Yagüe, A. et al., 2013, *Hot bottom burning and s-process nucleosynthesis in massive AGB stars at the beginning of the thermally-pulsing phase*, A&A, 555, L3
- Goodricke, J., 1786, *A series of observations on, and a discovery of, the period of the variation of the light of the star marked  $\delta$  by Bayer, near the head of Cepheus*, Philosophical Transactions of the Royal Society, 76, 48
- Greaves, J.S., & Holland, W.S., 1997, *High mass-loss carbon stars and the evolution of the local  $^{12}\text{C}/^{13}\text{C}$  ratio*, A&A, 327, 342
- Guzik, J.A., Jackiewicz, J. & Evans, R., 2023, *Challenges in Cepheid Evolution and Pulsation Modelling*, arXiv:2307.12386
- Hawkins, G., Mattei, J.A., & Foster, G., 2001, *R Centauri: An Unusual Mira Variable in a He-Shell Flash*, PASP, 113, 501
- Hertzsprung, E., 1926, Bull. Astron. Inst. Netherlands, 3, 115
- Herwig, F., 2005, *Evolution of Asymptotic Giant Branch Stars*, ARA&A, 43, 435
- Hoai, D.T., Winters, J.M., Nhung, P.T. et al., 2024, *Millimetre observations of the S-type AGB star chi Cygni: Variability of the emission of the inner envelope*, A&A, accepted. DOI: <https://doi.org/10.1051/0004-6361/202450983>
- Hoffleit, D., 1997, *History of the discovery of Mira stars*, Journal of AAVSO, 25, 115
- Homan, W., Pimpanuwat, B., Herpin, F. et al., 2021, *Atomium: The astounding complexity of the near circumstellar environment of the M-type AGB star R Hydrae. I. Morpho-kinematical interpretation of CO and SiO emission*, A&A, 651, A82
- Joyce, M. & Tayar, J., 2023, *A Review of the Mixing Length Theory of Convection in 1D Stellar Modelling*, Galaxies, 11/3, 75
- Joyce, M., Molnár, L., Cinquegrana, G. et al., 2024, *Stellar Evolution in Real Time. II. R Hydrae and an Open-Source Grid of >3000 Seismic TP-AGB Models Computed with MESA*, ApJ, 971, 186
- Kiss, L. L. & Szatmáry, K., 2002, *Period-doubling events in the light curve of R Cygni: Evidence for chaotic behaviour*, A&A, 390/2, 585
- Kudashkina, L.S. & Rudnitskij, G.M., 1994, *Influence of shock waves on the light curves of Long Period Variables*, Odessa Astron. Publ., 7, 66
- Lacour, S., Thiébaud, E., Perrin, G. et al., 2009, *The Pulsation of  $\chi$  Cygni Imaged by Optical Interferometry: A Novel Technique to Derive Distance and Mass of Mira Stars*, ApJ, 707/1, 632
- Leavitt, H.S., 1908, *1777 variables in the Magellanic Clouds*, Annals of the Astronomical Observatory of Harvard College, 60, 87
- Leavitt, H.S., 1912, *Periods of 25 variable stars in the Small Magellanic Cloud*, Harvard College Observatory Circular, 173, 1
- Le Bertre, T., 1992, *Carbon-star light curves in the 1-20  $\mu\text{m}$  range*, A&AS, 94, 377
- Lebzelter, T., Hinkle, K.H., Straniero, O., et al., 2019, *Carbon and Oxygen Isotopic Ratios. II. Semi-regular*

*Variable M Giants*, ApJ, 886, 117

Lebzelter, T., 2011, *The shapes of light curves of Mira-type variables*, Astron. Nachr., 332, 140

Liljegren, S., Höfner, S., Nowotny, W., & Eriksson, K., 2016, *Dust-driven winds of AGB stars: The critical interplay of atmospheric shocks and luminosity variations*, A&A, 589, A130

Lockwood, G. W., & Wing, R. F., 1971, *Light Curves of Mira Variables at 1.04 Micron*, ApJ, 169, 63

Loidl, R., Lançon, A. & Jørgensen, U.G., 2001, *Spectra of carbon-rich asymptotic giant branch stars between 0.5 and 2.5  $\mu\text{m}$ : Theory meets observation*, A&A, 371/3, 1065

Ludendorff, H., 1928, *Handbuch der Astrophysik*, 6/2, 49, Springer, Berlin

Marconi, M., De Somma, G., Molinaro, R. et al., 2022, *The Hertzsprung progression of Classical Cepheids in the Gaia era*, MNRAS, 529/4, 4210

Marigo, P., Bressan, A., Nanni, A., Girardi, L., & Pumo, M. L., 2013, *Evolution of thermally pulsing asymptotic giant branch stars - I. The COLIBRI code*, MNRAS, 434, 488

Marsakova, V.I. & Andronov, I.L., 2007, *Variability of long-period pulsating stars. iii. Changes in the parameters of humps at the ascending branch*, Astrophysics, 50/1

Mayer, A., Jorissen, A., Kerschbaum, F. et al., 2013, *Large-scale environments of binary AGB stars probed by Herschel. I. Morphology statistics and case studies of R Aquarii and W Aquilae*, A&A, 549, A69

McDonald, I., De Beck, E., Zijlstra, A.A., & Lagadec, E., 2018, *Pulsation-triggered dust production by asymptotic giant branch stars*, MNRAS, 481, 4984

McDonald, I & Zijlstra, A.A., 2016, *Pulsation-triggered mass loss from AGB stars: the 60 day critical period*, ApJL, 823, L38

Mennessier, M.O., Boughaleb, H. & Mattei, J.A., 1997, *Mean light curves of long-period variables and discrimination between carbon- and oxygen-rich stars*, Astron. Astrophys. Suppl. Ser., 124/1, 143

Merchán Benítez, P., & Jurado Vargas, M., 2000, *Strong period decrease in the Mira star S Sex: a possible helium-shell flash*, A&A, 353, 264

Merchán Benítez, P., & Jurado Vargas, M., 2002, *S Orionis: A Mira-type variable with a marked period decrease*, A&A, 386, 244

Merchán-Benítez, P., Uttenthaler, S. and Jurado-Vargas, M., 2023, *Meandering periods and asymmetries in light curves of Miras: Observational evidence for low mass-loss rates*, A&A 672, A165

Miller Bertolami, M.M., 2016, *New models for the evolution of post-asymptotic giant branch stars and central stars of planetary nebulae*, A&A, 588, A25

Molnár, L., Joyce, M., & Kiss, L.L., 2019, *Stellar Evolution in Real Time: Models Consistent with the Direct Observation of a Thermal Pulse in T Ursae Minoris*, ApJ, 879, 62

Ohnaka, K., & Tsuji, T., 1996, *Quantitative analysis of carbon isotopic ratios in carbon stars. I. 62 N-type and 15 SC-type carbon stars*, A&A, 310, 933

Onaka, T., de Jong, T., Willems, F.J., 1989, *A study of M Mira variables based on IRAS LRS observations. I. Dust formation in the circumstellar shell*, A&A 218, 169

Paladini, C., Baron, F., Jorissen, A. et al., 2018, *Large granulation cells on the surface of the giant star  $\pi 1$  Gruis*, Nature, 553, 310

Pigott, E., 1785, *Observations of a new variable star*, Philosophical Transactions of the Royal Society, 75, 127

Prudil, Z., Dékány, I., Smolec, R. et al., 2020, *Humps and bumps: the effects of shocks on the optical light curves of fundamental-mode RR Lyrae stars*, A&A, 635, A66

Ramstedt, S., Montez, R., Kastner, J. et al., 2012, *Searching for X-ray emission from AGB stars*, A&A, 543, A147

Ramstedt, S., & Olofsson, H., 2014, *The  $^{12}\text{C}/^{13}\text{C}$  ratio in AGB stars of different chemical type. Connection to the  $^{12}\text{C}/^{13}\text{C}$  ratio and the evolution along the AGB*, A&A, 566, A145

Rau, G., Hron, J., Paladini, C. et al., 2017, *The adventure of carbon stars. Observations and modelling of a set of C-rich AGB stars*, A&A, 600, A92

Reid, M.J. & Goldston, J.E., 2002, *How Mira variables change visual light by a thousand-fold*, ApJ, 568/2, 931

Rizzuti, F., Hirschi, R., Varma, V. et al., 2024, *Shell mergers in the late stages of massive star evolution: new insight from 3D hydrodynamic simulations*, MNRAS, 533/1, 687

Roberts, R., 2020, *R Cygni*, <https://www.aavso.org/lpv-month-may-2020-RCyg>

Rosales-Guzmán, A., Sanchez-Bermudez, J., Paladini, C. et al., 2024, *A new dimension in the variability of AGB stars: convection patterns size changes with pulsation*, *A&A*, 688, 124

Schöier, F. L., & Olofsson, H., 2000, *The  $^{12}\text{C}/^{13}\text{C}$ -ratio in cool carbon stars*, *A&A*, 359, 586

Schorr, F., 2016, <https://www.aavso.org/lpv-humps>

Schwarzschild, M., & Härm, R., 1967, *Hydrogen Mixing by Helium-Shell Flashes*, *ApJ*, 150, 961

Soszynski, I., Dziembowski, W.A., Udalski, A. et al., 2007, *The Optical Gravitational Lensing Experiment. Period–Luminosity Relations of Variable Red Giant Stars*, *Acta Astronomica*, 57, 201

Straniero, O., Abia, C. & Domínguez, I., 2023, *The carbon star mystery: 40 years later. Theory and observations*, *Eur. Phys. J. A*, 59, 17

Templeton, M.R., Mattei, J.A., & Willson, L.A., 2005, *Secular Evolution in Mira Variable Pulsations*, *AJ*, 130, 776

Templeton, M. & Willson, L.A., *Mira stars with double maxima: humps, bumps and resonances*, [https://www.aavso.org/sites/default/files/publications/staff\\_pubs/templeton\\_mira\\_humps\\_bumps.pdf](https://www.aavso.org/sites/default/files/publications/staff_pubs/templeton_mira_humps_bumps.pdf)

Uttenthaler, S. & Lebzelter, T., 2010, *Correlation between technetium and lithium in a sample of oxygen-rich AGB variables*, *A&A*, 510, A62

Uttenthaler, S., van Stiphout, K., Voet, K., et al., 2011, *The evolutionary state of Miras with changing pulsation periods*, *A&A*, 531, A88

Uttenthaler, S., Lebzelter, T., Busso, M., et al., 2012, *Lithium destruction and production observed in red giant stars*, arXiv: 1206.2759

Uttenthaler, S., Meingast, S., Lebzelter, T., et al., 2016a, *LX Cygni: A carbon star is born*, *A&A*, 585, A145

Uttenthaler, S., Greimel, R., & Templeton, M., 2016b, *Is the semi-regular variable RU Vulpeculae undergoing a helium-shell flash?*, *Astron. Nachr.*, 337, 293

Uttenthaler, S., McDonald, I., Bernhard, K. et al., 2019, *Interplay between pulsation, mass loss, and third dredge-up: More about Miras with and without technetium*, *A&A*, 622, A120

Uttenthaler, S., Shetye, S., Nanni, A. et al., 2024, *The impact of third-dredge-up on the mass loss of Mira variables*, *A&A*, 690, A393

Van Belle, G.T., Dyck, H.M., Benson, J.E. & Lacasse, M.J., 1996, *Angular size measurements of 18 Mira variable stars at 2.2  $\mu\text{m}$* , *Astronomical J.*, 112/5, 2147

Van Belle, G.T., Thompson, R.R. & Creech-Eakman, M.J., 2002, *Angular size measurements of Mira variable stars at 2.2 microns. II.*, *Astronomical J.*, 124, 1706

Vardya, M.S., 1987, *Shape of the visual light curve and detection of a 1.35 cm  $\text{H}_2\text{O}$  line in single M Miras*, *A&A* 182, 75

Vardya, M.S., deJong, T., Willems, F.J., 1986, *IRAS Low-Resolution Spectrograph Observations of Silicate and Molecular  $\text{SiO}$  Emission in Mira Variables*, *ApJ* 304, L29

Vardya, M. S., 1988, *Classification of Mira variables based on visual light curve shape*, *A&AS*, 73, 181

Walker, W.S.G., 2009, *BH Crucis : Period, Magnitude, and Color Changes*, *J. Am. Assoc. Variable Star Obs.*, 37/2, 87

Wallerstein, G., Hinkle, K.H., Dominy, J.F., 1985, *The spectrum of R Cygni during its exceptionally low maximum of 1983*, *MNRAS*, 215, 67

Whitelock, P. A., 1999, *"Real-time" evolution in Mira variables*, *New Astronomy Reviews*, 43, 437

Whitelock, P.A., Feast, M.W. & Van Leeuwen, F., 2008, *AGB variables and the Mira period–luminosity relation*, *MNRAS*, 386/1, 313

Winters, J.M., Fleischer, A.J., Gauger, A. and Sedlmayr, E., 1994, *Circumstellar dust shells around long-period-variables*, *A&A*, 290, 623

Wood, P.R., & Zarro, D.M., 1981, *Helium-shell flashing in low-mass stars and period changes in Mira variables*, *ApJ*, 247, 247

Wood, P.R. & Sebo, K.M., 1996, *On the pulsation mode of Mira variables: evidence from the Large Magellanic Cloud*, *MNRAS*, 282, 958

Woodruff, H.C., Tuthill, P.G., Monnier, J.D. et al., 2008, *The Keck Aperture Masking Experiment:*

- Multiwavelength Observations of Six Mira Variables*, ApJ, 673/1, 418
- Zhao-Geisler, R., Quirrenbach, A., Köhler, R. & Lopez, B., 2012, *Dust and molecular shells in asymptotic giant branch stars*, A&A, 545, A56
- Zhevakin, S. A., 1953, *Kappa Theory of Cepheids*, Astronom. Journal, 30, 161
- Zijlstra, A.A., Bedding, T.R., & Mattei, J.A., 2002, *The evolution of the Mira variable R Hydrae*, MNRAS, 334, 498
- Zijlstra, A.A., & Bedding, T.R., 2002, *Period Evolution in Mira Variables*, JAAVSO, 31, 2
- Zijlstra, A.A., Bedding, T.R., Markwick, A.J., 2004, *Period and chemical evolution of SC stars*, MNRAS, 352/1, 325

## Appendix

Table A1. Parameters of the 71 curves of sample A. Columns 2 ( $P/dP/P$ ), 3 ( $K-[22]/[3.4]-[22]$ ), 6 (spectral type) and 7 ( $^{12}\text{C}/^{13}\text{C}$  ratio) are copied from Merchán Benítez et al. (2023). Columns 4 (asymmetry parameter  $\alpha$ , in %), 5 (irregularity parameters  $\Delta M_{max}$  and  $\Delta' M_{max}$ , in units of 0.01 mag), 8 (oscillation amplitude  $A$ , in mag), 9 (Merchán Benítez index  $K_{MB}$ ), 10 (full width at half maximum of the oscillation profile in units of period,  $W_{1/2}$ ) and 11 (profile type) are evaluated approximately as described in Sections 2 and 3. The curves are ranked by alphabetic order in each of the four spectral-type families, Mno, Myes, S and C.

Name	$P/dP/P$	$K-[22]$ [3.4]-[22]	$\alpha$	$\Delta M_{max}/$ $\Delta' M_{max}$	Type	$^{12/13}\text{C}$	$A$	$K_{MB}$	$W_{1/2}$	Profile
R Aql	281/17	2.3/2.2	-7	36/38	Mno	8	5.0	-0.6	45	a
R Boo	224/2	1.6/1.8	-10	30/38	Mno	-	5.5	-0.5	45	a
R Cas	431/2	2.4/1.8	-25	75/99	Mno	12	6.5	1.0	45	b
X Crb	241/3	1.6/1.8	-7	33/38	Mno	-	4.5	-0.3	44	a
R Del	286/2	1.8/1.5	-14	35/41	Mno	-	4.5	-0.4	39	a
W Dra	279/15	3.0/2.4	-18	49/51	Mno	-	5.0	-1.3	51	a
T Her	165/2	1.3/1.6	-13	40/50	Mno	-	5.0	-0.9	49	a
U Her	406/2	2.4/2.5	-20	36/41	Mno	19	4.5	0.7	45	b
S Lac	240/3	2.1/1.9	-7	29/39	Mno	-	4.5	-0.8	44	a
R Leo	312/3	1.3/1.0	-13	37/47	Mno	10	5.0	0.8	38	b
R LMi	373/2	3.0/2.4	-19	56/66	Mno	12	5.0	-0.3	41	b
R Tri	267/1	1.8/1.5	-11	32/39	Mno	-	5.7	-0.2	44	a
T Uma	256/2	2.4/2.3	-20	50/69	Mno	-	5.5	-1.0	47	a
U Ari	372/2	2.1/2.1	-26	57/61	Myes	-	6.2	0.6	44	a
R Aur	457/4	2.4/1.8	5	42/53	Myes	33	6.0	1.3	62	d
T Cep	390/7	1.2/1.2	5	28/29	Myes	33	4.5	1.7	59	c
S CMi	333/2	2.0/1.7	-1	31/27	Myes	18	5.2	0.3	59	d
V CMi	366/2	2.5/2.0	-17	76/101	Myes	-	6.0	0.2	35	a
V Gem	275/5	1.5/1.5	-14	48/53	Myes	-	6.7	0.2	45	a
RU Her	486/5	2.2/2.4	-11	60/78	Myes	25	6.5	1.8	34	b
S Her	306/5	1.0/1.2	-2	32/39	Myes	-	5.5	1.0	58	d
R Hor	405/3	2.4/1.8	-21	46/53	Myes	-	7.0	0.7	43	a
R Hya	388/15	0.8/0.9	7	32/26	Myes	26	3.5	2.1	55	c
S Ori	424/9	1.7/1.9	3	41/23	Myes	45	5.0	1.6	48	c
Z Peg	328/4	1.6/1.7	0	28/33	Myes	-	5.0	0.6	45	-
R Ser	356/2	1.9/2.0	-20	49/67	Myes	14	7.0	0.6	42	a
S Vir	378/3	2.0/1.9	-12	35/48	Myes	-	6.2	0.8	41	b
R And	410/3	2.9/2.3	-24	77/71	Syes	40	7.0	0.2	46	a
RR And	328/2	1.3/1.2	-6	47/52	S?	-	6.0	0.9	53	a/-
W And	396/2	1.8/1.8	-20	73/91	Syes	-	6.5	1.2	38	b
X And	346/2	2.2/2.1	-26	39/47	S?	-	5.5	0.2	42	a
W Aql	487/3	3.0/3.4	-25	102/58	Syes	26	6.0	1.0	44	a
R Cam	270/4	0.2/0.6	-3	29/23	S?	-	5.0	1.4	57	d
T Cam	374/4	0.8/0.5	-3	18/14	Syes	31	5.5	1.9	63	d
S Cas	613/3	4.1/3.1	-20	65/51	S?	32	6.0	1.3	34	b
U Cas	277/2	1.3/1.0	-11	31/37	S?	-	6.5	0.4	48	a
WY Cas	479/1	3.6/2.8	-23	58/54	Syes	-	6.0	0.3	38	b
SZ Cep	329/2	2.0/1.5	-8	50/34	S?	-	5.5	0.2	49	d
V Cnc	272/2	1.8/1.0	-17	33/36	Syes	-	5.0	-0.2	57	a
Chi Cyg	408/2	2.4/1.7	-17	71/96	Syes	36	9	0.7	49	c
FF Cyg	325/2	0.9/1.0	-9	21/19	S?	-	4.5	1.3	62	d
R Cyg	427/2	2.9/2.9	-29	92/144	Syes	29	5/8	0.4	49	a
S Cyg	323/3	0.7/0.9	-4	49/67	S?	-	5-6	1.5	49	c
Z Del	305/2	1.6/1.2	-5	42/54	Syes	-	5.5	0.4	44	c
R Gem	370/2	1.9/2.0	-31	24/31	Syes	22	7.0	0.8	43	a
T Gem	289/4	0.1/0.8	-4	27/22	Syes	-	5.5	1.7	56	d
R Lyn	378/2	1.6/1.1	-14	44/44	Syes	-	6.0	1.2	53	d
T Sgr	393/4	1.7/1.2	-8	33/32	Syes	-	4.0	1.2	43	c
S Uma	226/4	1.2/1.1	-1	14/14	Syes	-	3.5	-0.1	58	d
AZ Aur	415/3	3.0/2.0	-10	68/51	Cyes	-	~3	0.2	50	-
UV Aur	395/1	3.0/2.5	-18	42/38	Cyes	-	2.2	0.0	48	-

V Aur	353/3	1.7/1.5	4	21/23	C?	-	2.5	0.8	48	a/-
S Cam	330/3	0.9/1.2	2	16/14	C?	14	2.0	1.4	65	d
W Cas	408/2	0.7/1.2	-5	22/19	Cyes	25	2.5	2.4	60	d/c
X Cas	424/4	1.6/1.3	10	29/22	C?	19	2	1.7	56	e/c
AX Cep	398/2	2.7/2.6	-10	79/51	C?	-	2.5	0.3	53	e/a
S Cep	484/3	2.7/1.7	6	47/50	C?	224	2.5	1.2	47	c
R Cmi	340/2	1.1/1.4	-12	46/34	Cyes	11	2.7	1.3	53	e/a
V Crb	358/4	2.3/1.9	-20	50/41	Cyes	-	3	0.3	45	a
BH Cru	529/10	1.6/1.4	-3	25/22	SCyes	8	3	2.8	65	c/e
U Cyg	463/5	1.9/2.2	-4	48/43	Cyes	14	3.0	1.8	47	c
V Cyg	421/2	3.2/2.3	-14	61/47	C?	20	3.5	0.1	45	a/e
WX Cyg	411/2	1.5/1.5	-7	20/21	Cyes	5	4.7	1.6	60	e/d
T Dra	422/4	3.4/2.6	-9	54/44	Cyes	24	3	-0.1	50	e/a
R Lep	427/5	3.0/2.0	-2	84/47	C?	34	~2	0.3	50	c/e
T Lyn	409/6	2.1/1.8	-10	53/37	C?	-	3	1.0	51	a/-
U Lyr	452/4	2.4/1.8	4	45/46	C?	23	~2	1.2	60	c/d
V Oph	297/4	1.6/1.4	-1	28/29	Cyes	11	2.5	0.3	63	d/e/a
RZ Peg	439/2	2.2/2.3	-16	36/40	Cyes	9	3.5	1.3	51	a/d
Y Per	249/4	1.6/1.1	10	23/21	C?	-	<=1	-0.2	70	-e
BD Vul	430/3	1.8/1.6	-1	46/52	C?	-	2.5	1.6	51	-e

Figure A1 below shows for each of the 32 light curves of sample B, from left to right, the mean normalised profile, the superimposed normalised profiles of the ascending branch, the rms deviation of each normalised pulse profile with respect to the mean normalised oscillation profile, the dependence on oscillation number of the period  $P$  (days), the amplitude  $A$  (mag) and the phase  $\phi_{min}$  as listed in Table 1 of the main text. The curves are ranked in alphabetic order for each spectral type separately, ending with the 8 additional M-type curves introduced in Section 4.4.

